

Numerical Stability Analysis of a Compressor Model

K. C. Reddy and Yeng-Yung Tsui
University of Tennessee Space Institute
Tullahoma, TN 37388

July 1982

Final Report of Period September 1, 1980 — December 1, 1981

Approved for public release; distribution unlimited.

**ARNOLD ENGINEERING DEVELOPMENT CENTER
ARNOLD AIR FORCE STATION, TENNESSEE
AIR FORCE SYSTEMS COMMAND
UNITED STATES AIR FORCE**

NOTICES

When U. S. Government drawings, specifications, or other data are used for any purpose other than a definitely related Government procurement operation, the Government thereby incurs no responsibility nor any obligation whatsoever, and the fact that the government may have formulated, furnished, or in any way supplied the said drawings, specifications, or other data, is not to be regarded by implication or otherwise, or in any manner licensing the holder or any other person or corporation, or conveying any rights or permission to manufacture, use, or sell any patented invention that may in any way be related thereto.

Qualified users may obtain copies of this report from the Defense Technical Information Center.

References to named commercial products in this report are not to be considered in any sense as an endorsement of the product by the United States Air Force or the Government.

This final report was submitted by University of Tennessee Space Institute under contract No. F40600-80-C-0006. Mr. Ross Roepke, Directorate of Technology was the Air Force project manager during this contract period.

This report has been reviewed by the Office of Public Affairs (PA) and is releasable to the National Technical Information Service (NTIS). At NTIS, it will be available to the general public, including foreign nations.

APPROVAL STATEMENT

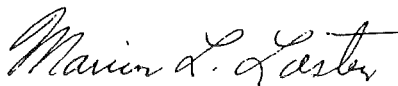
This report has been reviewed and approved.



ROSS G. ROEPKE
Directorate of Technology
Deputy for Operations

Approved for publication:

FOR THE COMMANDER



MARION L. LASTER
Director of Technology
Deputy for Operations

UNCLASSIFIED

SECURITY CLASSIFICATION OF THIS PAGE (When Data Entered)

REPORT DOCUMENTATION PAGE		READ INSTRUCTIONS BEFORE COMPLETING FORM
1. REPORT NUMBER AEDC-TR-82-16	2. GOVT ACCESSION NO.	3. RECIPIENT'S CATALOG NUMBER
4. TITLE (and Subtitle) NUMERICAL STABILITY ANALYSIS OF A COMPRESSOR MODEL		5. TYPE OF REPORT & PERIOD COVERED Final Report Sept. 1, 1980-Dec. 1, 1981
		6. PERFORMING ORG. REPORT NUMBER UTSI Report No. 82-5
7. AUTHOR(s) K. C. Reddy and Yeng-Yung Tsui		8. CONTRACT OR GRANT NUMBER(s) F40600-80-C-0006
9. PERFORMING ORGANIZATION NAME AND ADDRESS University of Tennessee Space Institute Tullahoma, TN 37388		10. PROGRAM ELEMENT, PROJECT, TASK AREA & WORK UNIT NUMBERS
11. CONTROLLING OFFICE NAME AND ADDRESS Arnold Engineering Development Center/DOS Air Force Systems Command Arnold Air Force Station, TN 37389		12. REPORT DATE July 1982
14. MONITORING AGENCY NAME & ADDRESS (if different from Controlling Office)		13. NUMBER OF PAGES 64
		15. SECURITY CLASS. (of this report) UNCLASSIFIED
		15a. DECLASSIFICATION/DOWNGRADING SCHEDULE NA
16. DISTRIBUTION STATEMENT (of this Report) Approved for public release; distribution unlimited.		
17. DISTRIBUTION STATEMENT (of the abstract entered in Block 20, if different from Report)		
18. SUPPLEMENTARY NOTES		
19. KEY WORDS (Continue on reverse side if necessary and identify by block number) compressor model JRS scheme numerical stability method of characteristics MacCormack scheme boundary conditions Runge-Kutta scheme		
20. ABSTRACT (Continue on reverse side if necessary and identify by block number) Various numerical schemes for solving the equations of a compressor model are analyzed. Runge-Kutta scheme, JRS scheme and MacCormack scheme have been studied. Proper imposition of the boundary conditions has been found to be critical for the numerical stability of these schemes. An accurate method of prescribing the boundary conditions by the use of characteristics has been developed. With this method of boundary conditions numerically stable results have been obtained for different test cases by all three numerical schemes.		

UNCLASSIFIED

SECURITY CLASSIFICATION OF THIS PAGE(When Data Entered)

They all predict the compressor surge with reasonable accuracy as compared to each other and in comparison with the experiments. It has been concluded that the MacCormack scheme with the boundary conditions based on the method of characteristics is the best overall scheme for compressor model predictive calculations.

UNCLASSIFIED

SECURITY CLASSIFICATION OF THIS PAGE(When Data Entered)

PREFACE

The work reported herein was conducted at the University of Tennessee Space Institute, Tullahoma, Tennessee, and was supported by the Arnold Engineering Development Center under Contract Number F40600-80-C-0006 for the period September 1, 1980 - December 1, 1981. The Air Force project manager during this contract period was Mr. Ross Roepke, Directorate of Technology.

The reproducibles used in the reproduction of this report were supplied by the authors: K. C. Reddy and Y.Y. Tsui.

TABLE OF CONTENTS

	<u>Page</u>
I. INTRODUCTION	7
II. COMPRESSOR MODEL AND THE BOUNDARY CONDITIONS	10
III. NUMERICAL SCHEMES	
A. Runge-Kutta Scheme	14
B. JRS (Jameson, Rizzi, and Schmidt) Scheme	18
C. MacCormack Scheme	19
IV. TEST CALCULATIONS	21
V. CONCLUSIONS	25
REFERENCES	26

APPENDICES

A. Derivation of the Characteristics and Compatibility Equations	27
B. Boundary Conditions Based on the Method of Characteristics	32

ILLUSTRATIONS

Figure

1. Compression System and the Control Volumes	37
1. Concluded	38
2. Stability Region in the Complex Plane for Fourth Order Runge-Kutta Scheme. [μ is given by Equation (17)]	39
3. Predicted Surge Points in 87 percent Corrected Speed Case	40

<u>Figure</u>		<u>Page</u>
4.	Model Prediction of the Compressor Performance under Loading till Surge Point at 86 percent Corrected Speed (Runge-Kutta Scheme)	41
5.	Model Prediction of the Compressor Performance under Loading till Surge Point at 87 percent Corrected Speed (JRS Scheme)	42
6.	Model Prediction of the Compressor Performance under Loading till Surge Point at 87 percent Corrected Speed (MacCormack Scheme)	43
7.	Variation of the Compressor Flow Parameters with Time till Surge Point - 87 percent Corrected Speed (Runge-Kutta Scheme)	44
8.	Variation of the Compressor Flow Parameters with Time till Surge Point - 87 percent Corrected Speed (JRS Scheme)	45
9.	Variation of the Compressor Flow Parameters with Time till Surge Point 87 percent Corrected Speed (MacCormack Scheme)	46
10.	Individual Stage Pressure Variations just before Surge - 87 percent Corrected Speed (Runge-Kutta Scheme)	47
11.	Individual Stage Pressure Variations just before Surge - 87 percent Corrected Speed (JRS Scheme)	48
12.	Individual Stage Pressure Variations just before Surge - 87 percent Corrected Speed (MacCormack Scheme)	49
13.	Individual Stage Airflow Variations just before Surge - 87 percent Corrected Speed (Runge-Kutta Scheme)	50
14.	Individual Stage Airflow Variations just before Surge - 87 percent Corrected Speed (JRS Scheme)	51

<u>Figure</u>		<u>Page</u>
15.	Individual Stage Airflow Variations just before Surge - 87 percent Corrected Speed (MacCormack Scheme)	52
16.	Model Prediction of the Compressor Performance under Loading till Surge Point at 102 percent Corrected Speed (Runge-Kutta Scheme)	53
17.	Model Prediction of the Compressor Performance under Loading till Surge Point at 102 percent Corrected Speed (JRS Scheme).	54
18.	Model Prediction of the Compressor Performance under Loading till Surge Point at 102 percent Corrected Speed (MacCormack Scheme)	55
19.	Variations of the Compressor Flow Parameters with Time till Surge Point - 102 percent Corrected Speed (Runge-Kutta Scheme)	56
20.	Variation of the Compressor Flow Parameters with Time till Surge Point - 102 percent Corrected Speed (JRS Scheme).	57
21.	Variation of the Compressor Flow Parameters with Time till Surge Point - 102 percent Corrected Speed (MacCormack Scheme)	58
22.	Individual Stage Pressure Variations just before Surge - 102 percent Corrected Speed (Runge-Kutta Scheme).	59
23.	Individual Stage Pressure Variations just before Surge - 102 percent Corrected Speed (JRS Scheme).	60
24.	Individual Stage Pressure Variations just before Surge - 102 percent Corrected Speed (MacCormack Scheme)	61
25.	Individual Stage Airflow Variations just before Surge - 102 percent Corrected Speed (Runge-Kutta Scheme)	62
26.	Individual Stage Airflow Variations just before Surge - 102 percent Corrected Speed (JRS Scheme).	63
27.	Individual Stage Airflow Variations just before Surge - 102 percent Corrected Speed (MacCormack Scheme)	64

I. INTRODUCTION

Aerodynamically stable operation of the compression system is vital in an aircraft turbine engine. A compressor delivers a desired quantity of airflow at a desired pressure level during the stable mode of operation. The aerodynamic stability limit line or surge line is the critical line on a compressor map which is a plot of the total pressure ratio across the compressor versus corrected airflow rate. Only below the surge line is the compressor stable. Compressor surge adversely affects engine performance by reducing engine airflow and thrust. The surge line is usually determined experimentally, based on steady-state and some limited unsteady data and various empirical correlations and corrections. The surge line, however, is affected by the fluctuations and distortions of the inlet flow and other transient phenomena during the operation of the system. Since it is not feasible to experimentally evaluate a compressor or an engine under all possible conditions, mathematical models are built to simulate the operation of compression systems.

Kimzey⁽¹⁾ developed a one-dimensional time-dependent model for the analysis of the effects of planar disturbances on a compressor system on the basis of conservation laws of mass, momentum and energy. Experimental data are used to synthesize the stage characteristics of the compressor. The compressor stage force and shaft work which are needed in the model are calculated based on these characteristics. Other factors such as the force of compressor casing acting on the fluid, heat added to the fluid and compressor bleed flow rate are also included in the model equations. The conservation equations are discretized spatially by the use of a two-sided difference scheme. Boundary conditions are imposed on total pressure and total temperature at the inlet boundary and on static pressure or airflow rate at the exit boundary. The resulting system of ordinary differential equations are integrated forward in time by a fourth-order Runge-Kutta scheme.

These models have been applied to a variety of compression systems by Kimzey⁽¹⁾ and Chamblee, Davis and Kimzey⁽²⁾. They are used to analyze and extrapolate the experimental data and to study the effects of unsteady disturbances on the aerodynamic stability of the compression system. These models are not always numerically stable. Some of the techniques used for overcoming the numerical instabilities are to increase the friction coefficient in the inlet and exit ducting, altering the ducting lengths or areas and time averaging the numerical solutions once every few time steps. However, these techniques can achieve only conditional numerical stability for some of the compression systems. Also the application of the models has been restricted to limited regions of the operating map. For certain regions of the operating map the models are numerically unstable.

Davis⁽³⁾ has applied the MacCormack's explicit finite difference scheme to solve the partial differential equations of the model and an approximate version of the method of characteristics to impose the boundary conditions. This scheme is more stable numerically than the earlier method, but this also exhibits numerical oscillations in the solutions under certain conditions. These oscillations are controlled or reduced by the addition of extra friction or dissipation in the inlet duct. However, the additional extra friction may degrade the accuracy of the simulation of the actual physical system.

In this report we present a study of the numerical stability of the compressor model and develop different schemes of enhanced numerical stability. The following items are discussed.

- a. mathematical study of the compressor model equations and the boundary conditions (application of the method of characteristics for imposing the boundary conditions accurately)
- b. numerical schemes and their stability characteristics:
 1. Runge-Kutta Scheme
 2. JRS (Jameson, Rizzi, Schmidt) Scheme
 3. MacCormack Scheme

c. stable test calculations using the AEDC data

The alternate methods of solution for the compressor model equations developed in this report have been shown to be numerically stable and are compared against each other and with some limited experimental data.

II. COMPRESSOR MODEL AND THE BOUNDARY CONDITIONS

The compression system modeled and the control volume system are shown in Fig. 1. The governing equations derived (1,2) by the application of the mass, momentum and energy conservation laws to the elemental control volume in Fig. 1-d in which blade forces, wall shear forces, shaft work done, heat added to the fluid and mass bleed flow rate are included. The resulting system of first order partial differential equations can be written as follows:

$$\frac{\partial \vec{u}(z,t)}{\partial t} + \frac{\partial \vec{f}}{\partial z}(\vec{u}) + \vec{g}(\vec{u}, z, t) = 0 \quad (1)$$

where

$$\vec{u}(z,t) = \begin{bmatrix} \rho A \\ \rho AU \\ \rho A \left(e + \frac{U^2}{2} \right) \end{bmatrix}, \quad \vec{f}(\vec{u}) = \begin{bmatrix} \rho AU \\ A (\rho U^2 + P) \\ \rho AU C_p T_t \end{bmatrix}$$

$$\vec{g}(\vec{u}, z, t) = \begin{bmatrix} W_B \\ -P \frac{\partial A}{\partial z} - F \\ -W_s - Q \end{bmatrix} \quad (2)$$

The various symbols represent the following:

- ρ = density
- A = area
- U = axial velocity
- e = internal energy
- P = static pressure
- C_p = specific heat at constant pressure
- T_t = stagnation temperature

- W_B = compressor bleed flow rate
 F = force of compressor blading and casing friction acting on the fluid
 W_S = stage shaft work added to fluid in control volume
 Q = rate of heat addition to control volume

In conjunction with the partial differential equations (1), we have the equation of state given by

$$P = \rho R T \quad (3)$$

where T is the static temperature and R the gas constant. In addition we have the equations relating the internal energy and stagnation temperature to other variables as follows:

$$e = C_p T / \gamma \quad (4)$$

$$C_p T_t = C_p T + \frac{U^2}{2} \quad (5)$$

The area distribution $A(z)$ is known for a given compressor system. In the vector \vec{g} , which acts like a forcing function in the differential equation, various terms are modeled empirically for a particular compressor except perhaps the pressure term which may be computed as a part of the solution. $F(z,t)$ represents the forces of the blades and the casing friction acting on the fluid. In practice it is difficult to isolate $F(z,t)$ empirically from the experimental data and hence the total term $(F + P \partial A / \partial z)$ which represents the forces including the wall pressure area force is modeled from the experimental data. $W_s(z,t)$ is the shaft work done on the fluid, which depends on the stage characteristics of the compressor. The stage characteristics are modeled empirically based on experimental measurements of stage total temperature, flow rate, total pressure and flow angularity at the stage entry and exit, and are corrected to account for unsteady flows through cascades based on the work of Goethert and Reddy⁽⁴⁾.

$Q(z,t)$ is the heat addition to the fluid and $W_B(z,t)$ is the bleed flow distribution function which models the mass removal or addition between stages.

The equations (1) can be written in the quasi-linear form

$$\frac{\partial \vec{u}}{\partial t} + M(\vec{u}) \frac{\partial \vec{u}}{\partial z} + \vec{g}(\vec{u}, z, t) = 0 \quad (6)$$

where $M(\vec{u}) = \frac{\partial \vec{f}}{\partial \vec{u}}$ is called the Jacobian Matrix of the system. As it is shown in the Appendix A, the Jacobian matrix M has three real and distinct eigenvalues U , $U+c$, $U-c$, where c is the speed of sound. Hence the system of partial differential equations (1) is hyperbolic. According to the theory of hyperbolic partial differential equations⁽⁵⁾, the number of boundary conditions to be imposed on the left boundary should equal the number of positive eigenvalues of M , which in the present case is two for subsonic incoming flows. In other words there are two incoming characteristics at the inlet for subsonic flows and correspondingly we need to impose two boundary conditions there. Similarly on the right boundary, the number of boundary conditions to be imposed should equal the number of negative eigenvalues of M there. For subsonic outflows, as is the case in the present model, we have one negative eigenvalue, $U-c$, which corresponds to one incoming characteristic at the outflow boundary and we impose one right boundary condition. In the present model, we prescribe the total pressure $P_t(t)$ and the total temperature $T_t(t)$ at the left boundary and the static pressure $P(t)$ or the mass flow rate $W(t)$ at the right boundary.

Since it is a hyperbolic system, the best way to formulate three other conditions at the boundaries, which may be necessary in numerical computations is by the method of characteristics. The following three compatibility equations along the three characteristic directions are derived in Appendix A. These equations are equivalent to the original system of partial differential equations.

$$c^2 \frac{d\bar{\rho}}{dt} - \frac{d\bar{P}}{dt} + c^2 \tilde{g}_1 - \tilde{g}_3 = 0 \text{ along } \frac{dz}{dt} = U \quad (7)$$

$$\bar{\rho}c \frac{dU}{dt} + \frac{d\bar{P}}{dt} + \bar{\rho}c \tilde{g}_2 + \tilde{g}_3 = 0 \text{ along } \frac{dz}{dt} = U+c \quad (8)$$

$$-\bar{\rho}c \frac{dU}{dt} + \frac{d\bar{P}}{dt} - \bar{\rho}c \tilde{g}_2 + \tilde{g}_3 = 0 \text{ along } \frac{dz}{dt} = U-c \quad (9)$$

where the quantities \tilde{g}_1 , \tilde{g}_2 , \tilde{g}_3 are defined in the Appendix A.

The first two characteristic curves, corresponding to the eigenvalues U and $U+c$ are the so-called right-running characteristics and the third one corresponding to $U-c$ is the left-running characteristic. We have two boundary conditions and one compatibility equation (9) at the inflow boundary and one boundary condition and two compatibility equations (7) and (8) at the outflow boundary. These equations are sufficient to solve for all the flow variables at the boundaries necessary for the interior point numerical schemes considered in this report. An accurate iterative method is used to solve these equations on the boundaries. Details are given in the Appendix B.

III. NUMERICAL SCHEMES

Three different numerical schemes, namely the Runge-Kutta Scheme, the JRS (Jameson, Rizzi and Schmidt) Scheme and the MacCormack Scheme have been used to integrate the partial differential equations forward in time. All of the schemes are explicit. In the JRS and the Runge-Kutta Schemes, the spatial derivatives are approximated by second-order accurate two-sided differences, while in the MacCormack Scheme forward and backward differences are used in two steps which also yield second order accuracy.

A. RUNGE-KUTTA SCHEME

The partial differential equations (1) can be rewritten as

$$\left(\frac{\partial \vec{u}}{\partial t}\right)_i = -\left(\frac{\partial \vec{f}}{\partial z} + \vec{g}\right)_i \quad (10)$$

where i is the interior point index. The spatial derivatives on the right are approximated by second-order accurate two-sided differences. The resulting set of ordinary differential equations are of the form:

$$\left.\frac{d\vec{u}}{dt}\right|_i = \vec{F}(\vec{u}_{i-1}, \vec{u}_i, \vec{u}_{i+1}, t) \quad i = 2, \dots, I-1 \quad (11)$$

where the index $i = 1$ corresponds to the left boundary and the index $i = I$ to the right boundary.

The equations (11) are integrated forward in time by a fourth order accurate (in time) Runge-Kutta Scheme:

$$\vec{u}^{n+1} = \vec{u}^n + \frac{1}{6} (\vec{k}_1 + 2\vec{k}_2 + 2\vec{k}_3 + \vec{k}_4) \quad (12)$$

where

$$\vec{k}_1 = \Delta t \vec{F}(\vec{u}^n, t_n)$$

$$\vec{k}_2 = \Delta t \vec{F}(\vec{u}^n + \vec{k}_1/2, t_n + \Delta t/2)$$

$$\vec{k}_3 = \Delta t \vec{F} (\vec{u}^n + \vec{k}_2/2, t_n + \Delta t/2)$$

$$\vec{k}_4 = \Delta t \vec{F} (\vec{u}^n + \vec{k}_3, t_n + \Delta t)$$

The local linearized stability analysis (von-Neumann Stability) for the difference scheme (11) and (12) is carried out as follows. Since the non-homogeneous terms \vec{g} in the equations (1) or (6) are computed at each time step using some empirical models based on experimental data, we need only consider the homogeneous part

$$\frac{\partial \vec{u}}{\partial t} + M \frac{\partial \vec{u}}{\partial z} = 0 \quad (13)$$

where $M = \partial \vec{f} / \partial \vec{u}$ is the Jacobian matrix, for the purpose of numerical stability analysis. Even though we use non-uniform spatial steps in the numerical computations, we consider the central difference scheme with uniform mesh steps in the z-direction and constant (locally frozen) matrix M for the purpose of analysis. We can approximate (13) by

$$\frac{\partial \vec{u}_i}{\partial t} = M \frac{\vec{u}_{i+1} - \vec{u}_{i-1}}{2\Delta x} \quad (14)$$

We analyze how a Fourier wave component of the form $\vec{A}_k(t)e^{I k x}$, where $I = \sqrt{-1}$ and k is the wave number, is propagated in time by the difference equations. For a stable numerical scheme the magnitudes of the wave amplitudes should remain bounded for all frequencies of interest. Otherwise the numerical scheme is considered unstable. The time growth of a Fourier component of the solution with wave number k is obtained by seeking the solution of the equation (14) in the form

$$\vec{u}_i = \vec{A}_k(t) e^{I k i \Delta x}, \text{ where } I = \sqrt{-1} \quad (15)$$

Substituting \vec{u}_i in the equation (14) we obtain

$$\frac{d\vec{A}_k(t)}{dt} = I M \frac{\sin(k\Delta x)}{\Delta x} \vec{A}_k \quad (16)$$

where $0 \leq k \Delta x \leq \pi$. The limitation $k \Delta x \leq \pi$ is imposed by the fact that $k = \pi/\Delta x$ is the highest wave number that can be resolved by a finite difference scheme with mesh width Δx . The time growth of the amplitudes \vec{A}_k is thus governed by a linear system of ordinary differential equations (16). The coefficient matrix, $B = I M \sin(k\Delta x)/\Delta x$ of this system has three eigenvalues equal to $I \lambda \sin(k\Delta x)/\Delta x$, where λ represents the three eigenvalues of M , namely, U , $U-c$ and $U+c$. Since the eigenvalues of the coefficient matrix lie on the imaginary axis of the complex plane, the system of ordinary differential equations (16) is neutrally stable.

When a Runge-Kutta Scheme is used to integrate the system of ordinary differential equations (16), we can obtain the stability condition from the theory of numerical integration of ordinary differential equations.⁽⁶⁾ The eigenvalues, μ of the matrix $\Delta t B$ (Δt times the coefficient matrix) must lie within a zone of stability in the complex plane corresponding to the particular Runge-Kutta Scheme. The eigenvalues μ are given by

$$\mu = I \lambda \frac{\Delta t}{\Delta x} \sin(k\Delta x) \quad , \quad 0 \leq k\Delta x \leq \pi \quad (17)$$

where λ are the eigenvalues of M , namely, U , $U-c$, $U+c$. The stability zone in the complex plane corresponding to the fourth order Runge-Kutta Scheme is shown in Figure 2. The upper most point on the imaginary axis within the region of stability is approximately 2.7. Since all the three values of μ lie on the imaginary axis, the condition for stability is

$$\text{Max} \left| \lambda \frac{\Delta t}{\Delta x} \sin k\Delta x \right| \leq 2.7 \quad , \quad 0 \leq k\Delta x \leq \pi$$

This gives the necessary condition for stability in terms of the Courant number, CN as

$$\text{CN} = \text{Max} (U+c) \frac{\Delta t}{\Delta x} \leq 2.7 \quad (18)$$

Even if the time step Δt is chosen to satisfy the equation (18), stability is still marginal because the non-uniformness of the

mesh and the non-linearities in the convection terms can make μ to lie in the unstable region to the right of the imaginary axis of the complex plane. In fact, non-linear instabilities do occur with the Runge-Kutta scheme in practice. In the actual numerical calculations it has been found necessary to time average the solution once every 5 or 10 time steps to suppress the non-linear instabilities even after obeying the Courant number restriction. Those details are discussed in the section dealing with the results.

B. JRS (JAMESON, RIZZI AND SCHMIDT) SCHEME

This scheme proposed by Jameson, Rizzi and Schmidt⁽⁷⁾ is also based on two-sided spatial difference approximations of second order accuracy similar to the Runge-Kutta Scheme. It is a three-step method with one predictor and two corrector steps. Let D denote a second order accurate two-sided difference approximation for $\partial/\partial z$. The JRS Scheme can be written as follows:

$$\begin{aligned}
 P: \quad \overline{\vec{u}_i^{n+1}} &= \vec{u}_i^n - \Delta t (D\vec{f}_i^n + \vec{g}_i^n) \\
 C1: \quad \overline{\vec{u}_i^{n+1}} &= \vec{u}_i^n - \frac{1}{2} \Delta t (D\vec{f}_i^n + \vec{g}_i^n + D\overline{\vec{f}_i^{n+1}} + \overline{\vec{g}_i^{n+1}}) \\
 C2: \quad \vec{u}_i^{n+1} &= \vec{u}_i^n - \frac{1}{2} \Delta t (D\vec{f}_i^n + \vec{g}_i^n + D\overline{\vec{f}_i^{n+1}} + \overline{\vec{g}_i^{n+1}})
 \end{aligned} \tag{19}$$

The local stability analysis⁽⁷⁾ (von-Neumann stability analysis) of this scheme can be carried out by analyzing the growth of the amplitudes of the basic Fourier modes of the numerical solution from one time step to the next. Since the discretization in space and time are combined together in equation (19), we seek solutions of the form

$$\vec{u}_i^n = \vec{A}_k^n e^{Iki\Delta x}, \quad \text{where } I = \sqrt{-1} \tag{20}$$

For the purpose of linear stability analysis, the non-linear term \vec{Df}_i^n is replaced by $M \vec{Du}_i^n$ where M is the Jacobian matrix (frozen locally) and D is a central difference operator. Also the nonhomogeneous terms \vec{g} are dropped as mentioned before, since they do not influence the stability analysis. After some algebra, one can obtain a relation between the amplitudes at the n th and $(n+1)$ th time steps in the form

$$\vec{A}_k^{n+1} = G \vec{A}_k^n \quad (21)$$

where G is known as the amplification matrix. It can be shown that

$$G = (I - \bar{B} + \frac{1}{2} \bar{B}^2 - \frac{1}{4} \bar{B}^3) \quad (22)$$

where I is the identity matrix and $\bar{B} = I \Delta t M \sin(k\Delta x)/\Delta x$. Linear stability is assured if $\text{Max}|\text{eigenvalues of } G| \leq 1$.

$$\text{Eigenvalues of } G = 1 - \mu + \frac{1}{2} \mu^2 - \frac{1}{4} \mu^3 \quad (23)$$

where μ is given by the equation (17).

$$\begin{aligned} |\text{Eigenvalues of } G|^2 &= 1 - \frac{1}{4} v^4 (1 - \frac{1}{4} v^2) \\ &\leq 1, \text{ if } |v| \leq 2 \end{aligned} \quad (24)$$

where $v = \lambda \Delta t \sin(k\Delta x)/\Delta x$ and $\lambda = U, U-c$ or $U+c$. Thus the condition for linear stability is obtained as

$$CN = \text{Max} (U+c) \frac{\Delta t}{\Delta x} \leq 2 \quad (25)$$

The time accuracy of the scheme is of second order, which is less than that of the Runge-Kutta Scheme. However it requires less computing per time step while the time step can be taken nearly as large as that of the Runge-Kutta Scheme. However, this is also a non-dissipative scheme just like the Runge-Kutta Scheme and non-linear instabilities occur under certain conditions. For certain test runs it has been found necessary to time average the solutions once every 5 or 10 time steps.

C. MacCORMACK SCHEME

One of the most popular schemes for solving the time dependent Euler equations or Navier-Stokes equations is the MacCormack Scheme⁽⁸⁾ due to its many desirable features. It is a two-step, predictor-corrector method. In the predictor, the spatial derivatives are approximated by a backward difference scheme and in the corrector by a forward difference scheme. Although either the predictor or the corrector is only first order accurate in time and space, the total scheme, however, is second order accurate both in time and space. The scheme can be written as

$$\begin{aligned} \text{P: } \bar{u}_i^{n+1} &= \bar{u}_i^n - \frac{\Delta t}{\Delta z_i} (\bar{f}_i^n - \bar{f}_{i-1}^n) - \Delta t \bar{g}_i^n \\ \text{C: } \bar{u}_i^{n+1} &= \frac{1}{2} \left(\bar{u}_i^n + \bar{u}_i^{n+1} - \frac{\Delta t}{\Delta z_{i+1}} (\bar{f}_{i+1}^{n+1} - \bar{f}_i^{n+1}) - \Delta t \bar{g}_i^{n+1} \right) \end{aligned} \quad (26)$$

where $\Delta z_i = z_i - z_{i-1}$. Using an analysis similar to that outlined for the JRS scheme one can show that the necessary condition for local (linearized) stability of this scheme is that the Courant number, CN obey

$$\text{CN} = \max (U+c) \frac{\Delta t}{\Delta z} \leq 1 \quad (27)$$

MacCormack scheme is dissipative in the sense that the high frequency components of the errors are dissipated rapidly. Thus it is less susceptible to non-linear instabilities than the Runge-Kutta or JRS schemes. As a matter of fact whenever the Courant number is less than 1, the numerical calculations have always been stable without any time averaging. While the time step that can be chosen for this scheme is less than those of the Runge-Kutta and JRS schemes, the computation per step is less.

With the three difference schemes discussed above, the boundary conditions are imposed using the method of characteristics as discussed in the last section and the Appendix B. Test calculations have been performed using all the schemes and the

results are discussed in the next section. Simple extrapolation techniques at the boundaries have been found to be either unstable or otherwise unsatisfactory.

IV. TEST CALCULATIONS

The model described in the last two sections has been applied to a typical high-pressure compression system. A Schematic of this system is presented in Fig. 1-c which includes 4 inlet ducting control volumes, 10 compressor stage control volumes and 5 combustor control volumes. For the inlet ducting and combustor control volumes the friction force is calculated by $\tau_w = cf \rho v^2/2$ where cf is the assumed skin friction factor. The compressor blade force and the shaft work in each compressor stage are calculated from the corresponding stage characteristics⁽¹⁻²⁾. Compressor bleed flow rate and heat addition to the fluid are not considered in the test cases run. In the boundary conditions, the total pressure and the total temperature at the inlet are fixed, but the static pressure at the exit is specified as a function of time. The exit pressure is increased with time as a linear function (pressure ramp) at 50 psia/sec in one case and 20 psia/sec in another case. Computations have shown that the compressor surge occurs at about the same exit pressure level, as shown in Fig. 3. Hence, most of the computations have been done with 50 psia/sec exit pressure ramp.

For each run, the initial values of the dependent variables namely the density, the mass flow rate and the total energy are input at all the spatial locations of the grid. They can be obtained from another steady state code or can be empirically guessed. Force calculation data such as the stage characteristics are also input for a constant corrected speed. Time dependent calculations are done for a fraction of a second (0.1 sec in the present case) with fixed boundary conditions at both ends in order to reach a steady-state starting solution. At this point the exit static pressure is increased at a rate of 50 psia/sec. Test runs have been made with two different corrected speeds; one at 87 percent of design corrected speed and the other at 102 percent corrected speed.

A test case with 87 percent corrected speed has been run with $\Delta t = 0.00005$ which corresponds to the Courant number, $CN \approx 0.6$ using all three difference schemes. The Runge-Kutta scheme requires time-averaging of the solution once every 5 time steps in order to suppress the non-linear numerical instabilities. The numerical solution obtained by the JRS scheme exhibits some numerical oscillations but they are not severe enough to cause non-linear instability. However these numerical oscillations are removed by time-averaging the solution once every 5 time steps in the JRS scheme. The MacCormack Scheme produces stable solution without any numerical oscillations till the point of surge and does not require any time-averaging. The pressure ratio across the compressor is plotted against the percent corrected compressor inlet airflow in Figs. 4, 5, and 6 corresponding to the Runge-Kutta, JRS and MacCormack Schemes respectively. All these schemes produce the same performance map except near the surge point. The Runge-Kutta and JRS Schemes predict the surge point within 2 percent of the pressure ratio of the experimental surge point. The MacCormack scheme does it even better and predicts the surge point within 1 percent. Figures 7, 8 and 9 show the pressure ratio across the compressor and the percent corrected airflow against time till the point of surge, obtained by the three methods and they compare very well against each other.

In addition to the overall performance plots, we have also plotted some computed results of the individual stages. Figures 10, 11 and 12 show individual stage entrance static pressures against time and Figs. 13, 14 and 15 show the stage entrance airflow rate against time calculated by the three methods, just before the flow breaks down. At the time of compressor surge, the stage that initiates the surge will indicate a sudden increase in stage entrance pressure and a sudden decrease in exit pressure (which is the entrance pressure of the next stage). This signature is caused by flow stagnation at the entrance and recirculation at the stage exit, perhaps caused by flow separation on the blades.

By examining the individual stage pressure performance in the Figs. 10, 11 and 12, it may be inferred that the 2nd and 7th stages initiate the surge process. Experimental data, however, indicates that the surge is initiated at the 7th stage. It seems that the stage characteristic data for the 2nd stage, used in this test run, is not very accurate.

The model predictions of the compressor performance for the case of 102 percent corrected speed are given in Figs. 16 to 27. The experimental surge point for this case is at 100.4 percent corrected compressor inlet airflow when the pressure ratio across the compressor equals to 10. All three methods predict the surge point within 0.5 percent of the experimental values. Figures 22 to 24 indicate that the surge process is initiated at the 7th stage in this case. In general the model predictions in this case by the three methods agree with each other well and are better than the previous case. Experimental data agrees with the prediction of the 7th stage initiating the surge in this case.

We have made computations with larger time step ($\Delta t = 0.0001$) which corresponds to a Courant number $CN \approx 1.2$ to see if the runs can be speeded up. The Runge-Kutta and JRS Schemes with time-averaging yield same results as before for both 87 percent and 102 percent cases, but require only half the computing time. The MacCormack Scheme which is stable only for $CN \leq 1$, works even with $CN \approx 1.2$ for the 87 percent case and gives the same results as before in half the computing time. The MacCormack Scheme with $CN \approx 1.2$ becomes unstable for the 102 percent case, but can be stabilized however, by time-averaging the solution once every 2 time steps in which case it yields the same results as before again in half the computing time. In general it may be better to use the MacCormack method with $CN \approx 1.0$ and no time-averaging.

In conclusion the Runge-Kutta and JRS Schemes with time-averaging and the MacCormack Scheme without any time-averaging and the boundary conditions imposed with the use of characteristics in all the schemes yield numerically stable solutions of the

compressor model. Among the three schemes the MacCormack Scheme is preferred for its stability characteristics and efficiency in computation.

V. CONCLUSIONS

- A. The one-dimensional compressor model equations are hyperbolic and the imposition of proper boundary conditions is critical for solving them. For obtaining the numerical solutions of these equations, imposition of the boundary conditions based on the method of characteristics has been found to be the most accurate and stable technique.
- B. Three different finite difference schemes have been analyzed. The Runge-Kutta Scheme and the JRS (Jameson, Rizzi and Schmidt) Scheme exhibit non-linear instabilities even when the Courant number restriction is obeyed. However, both the schemes can be stabilized by time-averaging the solutions every 5 time steps. MacCormack Scheme has been found to yield numerically stable solutions without any time-averaging.
- C. All of the three difference schemes together with the boundary conditions based on the method of characteristics predict compressor surge reasonably accurately and agree with experimental data reasonably well for the test cases run. Overall, MacCormack Scheme has been found to be more accurate and reliable than the other two schemes.

REFERENCES

1. Kimzey, W. F. "An Analysis of the Influence of Some External Disturbances on the Aerodynamic Stability of Turbine Engine Axial-Flow Fans and Compressors". AEDC-TR-77-80 (AD-A043543), Aug. 1977.
2. Chamblee, C. E., Davis, M. W., Jr., and Kimzey, W. F. "A Multistage Axial-Flow Compressor Mathematical Modeling Technique with Application to Two Current Turbofan Compression Systems". AIAA Paper 80-0054 Presented at AIAA 18th Aerospace Sciences Meeting, Pasadena, CA, Jan. 14-16, 1980.
3. Davis, M.W., Jr. "A Stage-by-Stage Compressor Modeling Technique for Single and Dual-Spool Compression System". A Thesis presented for Master of Science Degree to the University of Tennessee, Aug. 1981.
4. Goethert, B. H., and Reddy, K.C. "Unsteady Aerodynamics of Rotor Blades of a Compressor Under Distorted Flow Conditions". Paper Presented at AGARD Fluid Dynamics Panel Specialist Meeting on Aerodynamic Interference, Silver Springs, Maryland, Sept. 28-30, 1970.
5. John, F. Partial Differential Equations. Springer-Verlag: New York, 1978.
6. Lapidus, L. and Seinfeld, J.H. Numerical Solution of Ordinary Differential Equations. Academic Press, New York, 1971.
7. Schmidt, W. "Transonic Potential Flow Computations and Explicit Methods for the Euler Equations". Lecture Notes of UTSI Short Course, Dec. 8-12, 1980.
8. MacCormack, R. W. "The Effect of Viscosity in Hypervelocity Impact Cratering." AIAA Paper 69-354, Cincinnati, OH, 1969.

APPENDIX A

DERIVATION OF THE CHARACTERISTICS
AND COMPATIBILITY EQUATIONS

The one-dimensional time-dependent compressor model equations in the conservation form, as given in equation (1) are

$$\frac{\partial \vec{u}(z,t)}{\partial t} + \frac{\partial \vec{f}(\vec{u})}{\partial z} + g(\vec{u}, z, t) = 0 \quad (A-1)$$

$$\vec{u} = \begin{bmatrix} \rho A \\ \rho AU \\ \rho A(e + \frac{U^2}{2}) \end{bmatrix} = \begin{bmatrix} \bar{\rho} \\ m \\ \epsilon \end{bmatrix}$$

$$f(\vec{u}) = \begin{bmatrix} \rho AU \\ A(\rho U^2 + P) \\ \rho AU(e + \frac{U^2}{2} + \frac{P}{\rho}) \end{bmatrix} = \begin{bmatrix} \bar{\rho} U \\ \bar{\rho} U^2 + \bar{P} \\ \bar{\rho} U(h + \frac{U^2}{2}) \end{bmatrix}$$

$$\vec{g}(\vec{u}, z, t) = \begin{bmatrix} g_1 \\ g_2 \\ g_3 \end{bmatrix}$$

where $\bar{\rho} = \rho A$, $m = \rho AU$, $\epsilon = \rho A(e + \frac{U^2}{2})$ are conservation variables and $\bar{P} = PA$, $h = e + \frac{P}{\rho}$. With the equation of state for perfect gas and calorically perfect gas assumption, the flux vectors \vec{f} can be rewritten in terms of the conservation variables:

$$\vec{f}(\vec{u}) = \begin{bmatrix} m \\ \frac{m^2}{\bar{\rho}} + (\gamma-1) \left[\epsilon - \frac{1}{2} \frac{m^2}{\bar{\rho}} \right] \\ m \left[\gamma \frac{\epsilon}{\bar{\rho}} + \frac{1-\gamma}{2} \frac{m^2}{\bar{\rho}} \right] \end{bmatrix}$$

Hence the Jacobian matrix

$$M = \frac{\partial \vec{f}}{\partial \vec{u}} = \begin{bmatrix} 0 & 1 & 0 \\ \frac{\gamma-3}{2} U^2 & (3-\gamma)U & \gamma-1 \\ -\gamma \frac{U\epsilon}{\bar{\rho}A} - (1-\gamma)U^3 & \gamma \frac{\epsilon}{\bar{\rho}A} + \frac{3}{2} (1-\gamma)U^2 & \gamma U \end{bmatrix}$$

The complexity of this Jacobian matrix makes it rather tedious to compute the eigenvalues. It is easier to work with the nonconservative or primitive variables $\tilde{u} = [\bar{\rho} \ u \ \bar{P}]^T$. We can rewrite the equation (A-1) as

$$L \frac{\partial \tilde{u}}{\partial t} + N \frac{\partial \tilde{u}}{\partial z} + \vec{g} = 0 \quad (A-2)$$

where

$$L = \frac{\partial \vec{u}}{\partial \tilde{u}} = \begin{bmatrix} 1 & 0 & 0 \\ U & \bar{\rho} & 0 \\ \frac{U^2}{2} & \bar{\rho}U & \frac{1}{\gamma-1} \end{bmatrix} \quad \text{and} \quad N = \frac{\partial \vec{f}}{\partial \tilde{u}} = \begin{bmatrix} U & \bar{\rho} & 0 \\ U^2 & 2\bar{\rho}U & 1 \\ \frac{U^3}{2} & \bar{\rho} \left(\frac{\gamma}{\gamma-1} \frac{\bar{P}}{\bar{\rho}} + \frac{3}{2} U^2 \right) & \frac{\gamma}{\gamma-1} U \end{bmatrix}$$

Multiplying the equation (A-2) by the inverse matrix L^{-1} , we convert it into a nonconservative form

$$\frac{\partial \tilde{u}}{\partial t} + \tilde{M} \frac{\partial \tilde{u}}{\partial z} + \tilde{g} = 0 \quad (A-3)$$

where

$$\tilde{M} = L^{-1} N = \begin{bmatrix} U & \bar{\rho} & 0 \\ 0 & U & \frac{1}{\bar{\rho}} \\ 0 & \gamma \bar{P} & U \end{bmatrix},$$

$$\tilde{g} = L^{-1} \vec{g} = \begin{bmatrix} g_1 \\ -\frac{U}{\bar{\rho}} g_1 + \frac{1}{\bar{\rho}} g_2 \\ \frac{(\gamma-1)}{2} U^2 g_1 + (1-\gamma) U g_2 + (\gamma-1) g_3 \end{bmatrix}$$

$$= \begin{bmatrix} \tilde{g}_1 \\ \tilde{g}_2 \\ \tilde{g}_3 \end{bmatrix}$$

and $\gamma \bar{P} = \bar{\rho} c^2$ where $c = \sqrt{\gamma R T}$ is the speed of sound. The non-conservative form matrix \tilde{M} is related to the Jacobian matrix M by the similarity transformation

$$\tilde{M} = L^{-1} M L$$

Therefore M and \tilde{M} have the same eigenvalues.

It is easy to derive the eigenvalues of \tilde{M} , which are U , $U+c$, $U-c$. The corresponding eigenvectors, written as column vectors, form the matrix

$$T = \begin{bmatrix} \frac{1}{c^2} & \frac{1}{2c^2} & \frac{1}{2c^2} \\ 0 & \frac{1}{2\bar{\rho}c} & -\frac{1}{2\bar{\rho}c} \\ 0 & \frac{1}{2} & \frac{1}{2} \end{bmatrix}$$

such that $T^{-1} \tilde{M} T = \Lambda$

where

$$T^{-1} = \begin{bmatrix} c^2 & 0 & -1 \\ 0 & \bar{\rho}c & 1 \\ 0 & -\bar{\rho}c & 1 \end{bmatrix} \quad \text{and} \quad \Lambda = \begin{bmatrix} U & 0 & 0 \\ 0 & U+c & 0 \\ 0 & 0 & U-c \end{bmatrix}$$

Multiplying the equation (A-3) by T^{-1} and using the similarity relation mentioned above, the following equation is obtained

$$T^{-1} \frac{\partial \tilde{u}}{\partial t} + \Lambda T^{-1} \frac{\partial \tilde{u}}{\partial z} + T^{-1} \tilde{g} = 0 \quad (\text{A-4})$$

This equation can be written in the scalar form as

$$c^2 \left(\frac{\partial}{\partial t} + U \frac{\partial}{\partial z} \right) \bar{\rho} - \left(\frac{\partial}{\partial t} + U \frac{\partial}{\partial z} \right) \bar{P} + c^2 \tilde{g}_1 - \tilde{g}_3 = 0 \quad (\text{A-5-1})$$

$$\bar{\rho}c \left(\frac{\partial}{\partial t} + (U+c) \frac{\partial}{\partial z} \right) U + \left(\frac{\partial}{\partial t} + (U+c) \frac{\partial}{\partial z} \right) \bar{P} + \bar{\rho}c \tilde{g}_2 + \tilde{g}_3 = 0 \quad (\text{A-5-2})$$

$$-\bar{\rho}c \left(\frac{\partial}{\partial t} + (U-c) \frac{\partial}{\partial z} \right) U + \left(\frac{\partial}{\partial t} + (U-c) \frac{\partial}{\partial z} \right) \bar{P} - \bar{\rho}c \tilde{g}_2 + \tilde{g}_3 = 0 \quad (\text{A-5-3})$$

These are called the compatibility equations in the characteristic directions. The characteristic directions S_1 , S_2 , S_3 are defined by

$$\frac{\partial}{\partial S_1} = \frac{\partial}{\partial t} + U \frac{\partial}{\partial z}, \quad \text{then} \quad \frac{dz}{dt} = U \text{ along } S_1 \quad (\text{A-6-1})$$

$$\frac{\partial}{\partial S_2} = \frac{\partial}{\partial t} + (U+c) \frac{\partial}{\partial z}, \quad \text{then} \quad \frac{dz}{dt} = U+c \text{ along } S_2 \quad (\text{A-6-2})$$

$$\frac{\partial}{\partial S_3} = \frac{\partial}{\partial t} + (U-c) \frac{\partial}{\partial z}, \quad \text{then} \quad \frac{dz}{dt} = U-c \text{ along } S_3 \quad (\text{A-6-3})$$

which are called the characteristic equations. Thus, in terms of the characteristic coordinates, the compatibility equations become

$$c^2 \frac{\partial \bar{\rho}}{\partial S_1} - \frac{\partial \bar{P}}{\partial S_1} + c^2 \tilde{g}_1 - \tilde{g}_3 = 0 \text{ along } S_1 \quad (\text{A-7-1})$$

$$\bar{\rho}c \frac{\partial U}{\partial S_2} + \frac{\partial \bar{P}}{\partial S_2} + \bar{\rho}c \tilde{g}_2 + \tilde{g}_3 = 0 \text{ along } S_2 \quad (\text{A-7-2})$$

$$-\bar{\rho}c \frac{\partial U}{\partial S_3} + \frac{\partial \bar{P}}{\partial S_3} - \bar{\rho}c \tilde{g}_2 + \tilde{g}_3 = 0 \text{ along } S_3 \quad (\text{A-7-3})$$

It may be noted that along each of these characteristic curves, the compatibility equations are ordinary differential equations and the parameters S_1 , S_2 , S_3 can be considered as time t itself. Thus we can rewrite the compatibility equations along the characteristics as follows:

$$c^2 \frac{d\bar{\rho}}{dt} - \frac{d\bar{P}}{dt} + c^2 \tilde{g}_1 - \tilde{g}_3 = 0 \text{ along } \frac{dz}{dt} = U \quad (\text{A-8-1})$$

$$\bar{\rho}c \frac{dU}{dt} + \frac{d\bar{P}}{dt} + \bar{\rho}c \tilde{g}_2 + \tilde{g}_3 = 0 \text{ along } \frac{dz}{dt} = U+c \quad (\text{A-8-2})$$

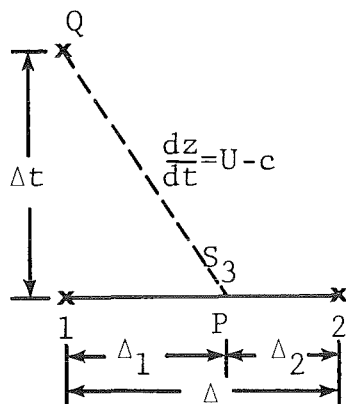
$$-\bar{\rho}c \frac{dU}{dt} + \frac{d\bar{P}}{dt} - \bar{\rho}c \tilde{g}_2 + \tilde{g}_3 = 0 \text{ along } \frac{dz}{dt} = U-c \quad (\text{A-8-3})$$

APPENDIX B

BOUNDARY CONDITIONS BASED ON THE
METHOD OF CHARACTERISTICS

1. Inlet Boundary

As mentioned in the main text, it is necessary and sufficient to impose two boundary conditions at the inlet boundary for subsonic inflows. In the present case the total pressure P_t and the total temperature T_t are prescribed at the inlet. For determining all the variables at the boundary point, however, we need another equation which is supplied by the compatibility equation along the characteristic direction S_3 .



In general, the location of P and the variables at Q will have to be solved iteratively. As an initial iteration, we approximate the characteristic S_3 by a straight line with the slope evaluated at P . $(U-c)$ at P is approximated by interpolation of its values at points 1 and 2. Location of P is thus obtained by solving the following three linear equations:

$$\Delta_1 + \Delta_2 = \Delta \quad (\text{B-1-1})$$

$$\Delta_1 = - (U-c)_P \Delta t \quad (\text{B-1-2})$$

$$(U-c)_P = [(U-c)_1 \Delta_2 + (U-c)_2 \Delta_1] / \Delta \quad (\text{B-1-3})$$

Then all the necessary thermodynamic variables at P can be determined by linear interpolation between points 1 and 2. The compatibility equation (A-8-3) is integrated from the point P to the point Q using a forward difference approximation, which can be written as

$$F(U_Q) = - \rho c (U_Q - U_P) + (P_Q - P_P) - \rho c \Delta t \tilde{g}_2 + \Delta t \tilde{g}_3 / A = 0 \quad (\text{B-2})$$

where U_Q and P_Q are unknowns and ρ and c are calculated at P in the initial iteration. Since the total pressure, P_t and the total temperature, T_t are prescribed at the point Q we can express P_Q in terms U_Q by the equation

$$P_Q = P_t \left[1 - \frac{U_Q^2}{2C_P T_t} \right]^{\frac{\gamma}{\gamma-1}} \quad (\text{B-3})$$

Using this equation, we can eliminate P_Q from the difference equation (B-2) and obtain the following nonlinear equation for U_Q .

$$F(U_Q) = - \rho c (U_Q - U_P) + P_t \left[1 - \frac{U_Q^2}{2C_P T_t} \right]^{\frac{\gamma}{\gamma-1}} - P_P - \rho c \Delta t \tilde{g}_2 + \Delta t \tilde{g}_3 / A = 0 \quad (\text{B-4})$$

Differentiating F, we can write

$$F'(U_Q) = - \rho c - \frac{\gamma}{\gamma-1} P_t \left[1 - \frac{U_Q^2}{2C_P T_t} \right]^{\frac{\gamma}{\gamma-1}-1} \left[\frac{U_Q}{C_P T_t} \right] \quad (\text{B-5})$$

The equation (B-4) is solved by the Newton-Raphson iteration:

$$U_Q^{(v+1)} = U_Q^{(v)} - F(U_Q^{(v)}) / F'(U_Q^{(v)}) \quad (B-6)$$

with the initial guess $U_Q^{(0)} = U_1$. This is the inner iteration within the outer iteration started earlier. The converged value for U_Q is the first iterate for U at Q . Further iterations are carried out to satisfy the compatibility equation to sufficient accuracy. This can be done by modifying the equation (B-1-2) as

$$\Delta_1 = - \frac{1}{2} [(U-c)_P + (U-c)_Q] \Delta t \quad (B-7)$$

where the latest values at P and Q are used in each iteration. Location of P is updated in each iteration and in the equations (B-4) and (B-5) ρ and c are calculated by the average of their values at P and Q :

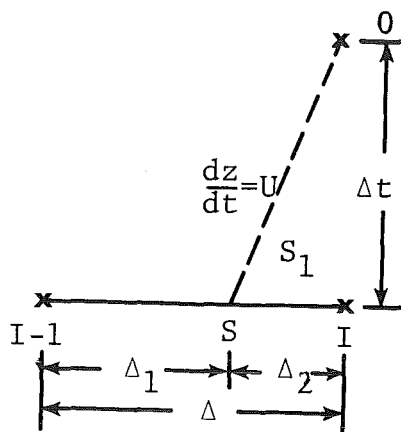
$$\rho = \frac{1}{2} (\rho_P + \rho_Q) \text{ and } c = \frac{1}{2} (c_P + c_Q) \quad (B-8)$$

This iterative process is continued till the values of U_Q converge. This convergence is usually obtained within 2 or 3 iterations at each time step. Once U_Q is known, all the other variables at Q can be computed.

2. Exit Boundary

For subsonic outflow, only one boundary condition can and should be imposed at the exit boundary. The static pressure P is prescribed at the exit in the present case. The other variables at the exit boundary point are determined by using the compatibility equations along the characteristic directions S_1 and S_2 .

a. Integration along the characteristic direction S_1 :



In a manner similar to the procedure used at the inlet boundary, the following three linear equations

$$\Delta_1 + \Delta_2 = \Delta \quad (\text{B-9-1})$$

$$\Delta_2 = U_S \Delta t \quad (\text{B-9-2})$$

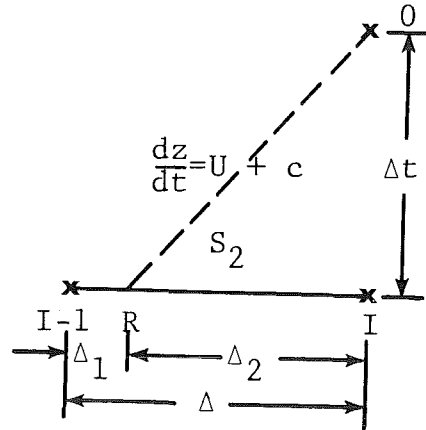
$$U_S = [U_{I-1} \Delta_2 + U_I \Delta_1] / \Delta \quad (\text{B-9-3})$$

are solved to determine the location of S and the thermodynamic properties of the flow at the point S are determined by a linear interpolation between the points I and (I-1). The compatibility equation (A-8-1) is integrated by a forward difference approximation and the density at the boundary point 0 is calculated by

$$\rho_0 = \rho_S + [P_0 - P_S - \Delta t (c^2 \tilde{g}_1 - \tilde{g}_3) / A] / c^2 \quad (\text{B-10})$$

where P_0 is known from the imposed boundary condition and all the coefficients are calculated at the point S.

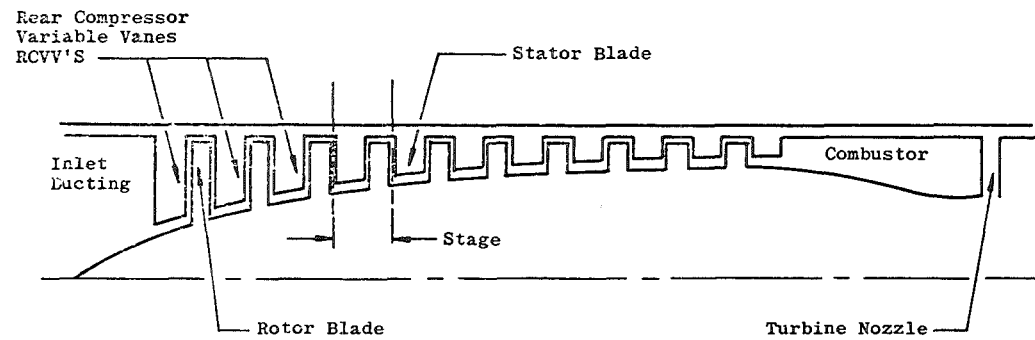
b. Integration along the characteristic direction S_3 :



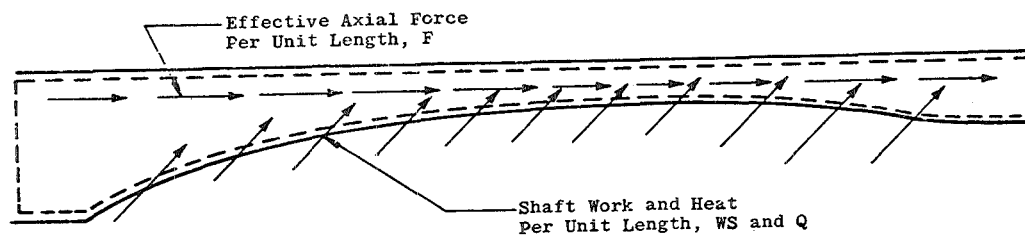
The same procedures as in case (a) is followed except that U in the equations (B-9-2) and (B-9-3) is replaced by $U+c$. The compatibility equation (A-8-2) is integrated to obtain U at the point 0 as

$$U_0 = U_R - [P_0 - P_R + \Delta t (\rho c \tilde{g}_2 + \tilde{g}_3/A)] / (\rho c) \quad (B-11)$$

The entire process of (a) and (b) can now be repeated by replacing U in the equation (B-9-2) and c in the equation (B-10) and ρc in the equation (B-11) by their respective averages at the points 0 and S or 0 and R. Convergence is usually achieved in 2 or 3 iterations. All the variables necessary at the exit boundary point 0 can now be determined.

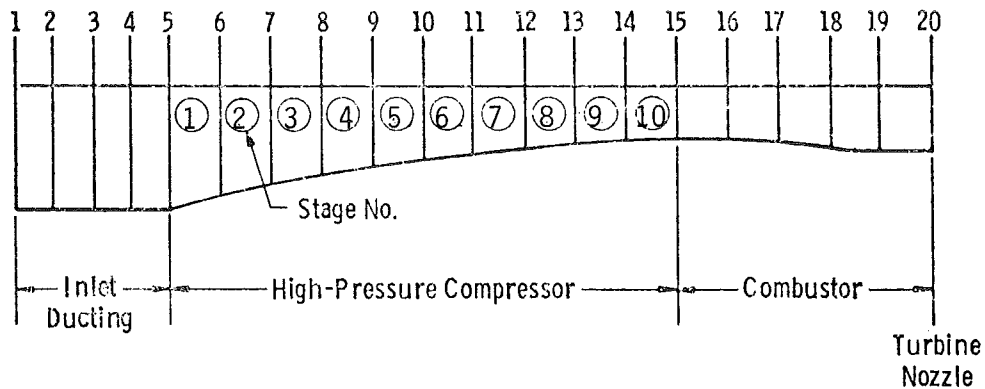


a. Physical high-pressure compressor modeled

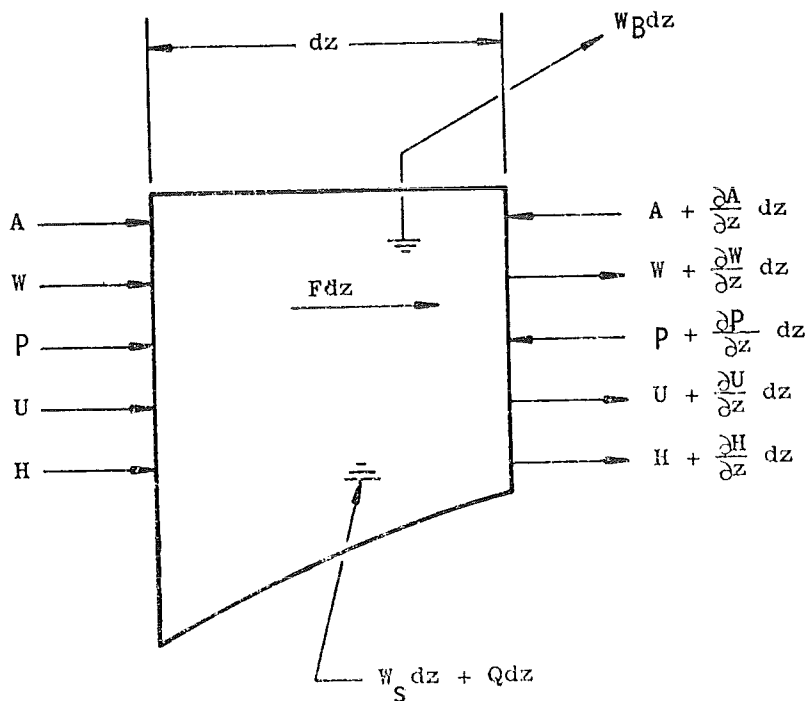


b. Overall control volume

Figure 1. Compression system and the control volumes.



c. Station locations



d. Elemental control volume
Figure 1. Concluded.

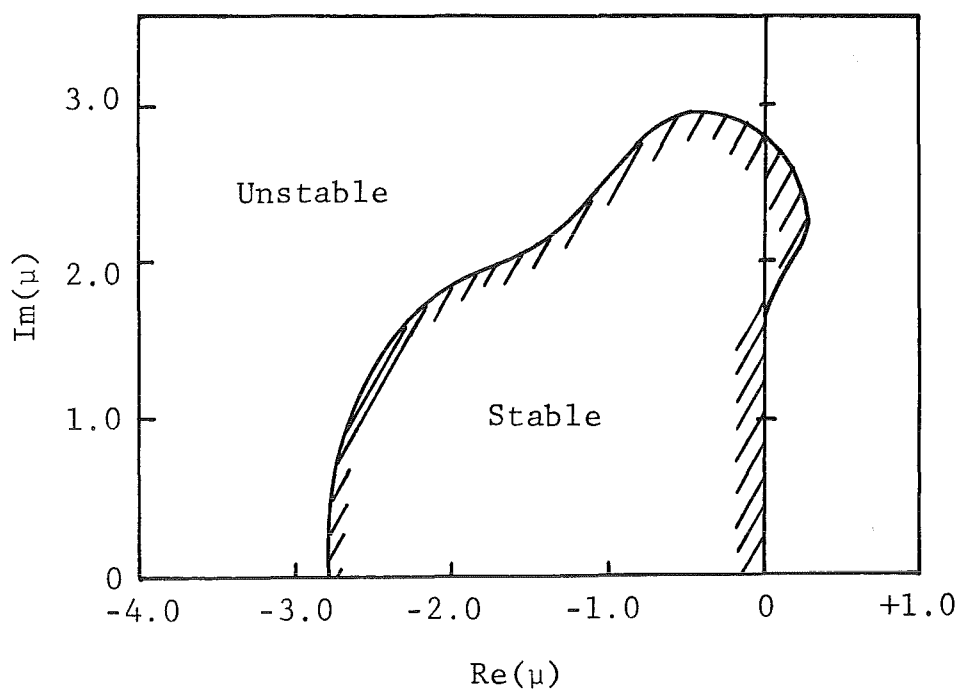


Figure 2. Stability region in the complex plane for fourth order Runge-Kutta Scheme.
[μ is given by Equation (17)]

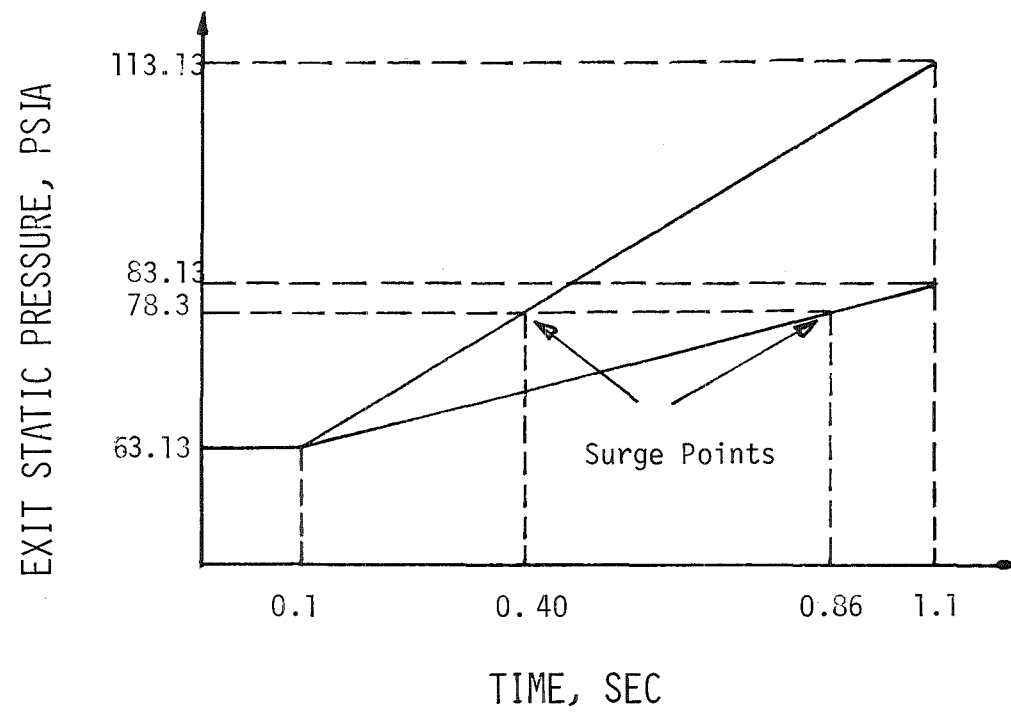


Figure 3. Predicted surge points in 87 percent corrected speed case.

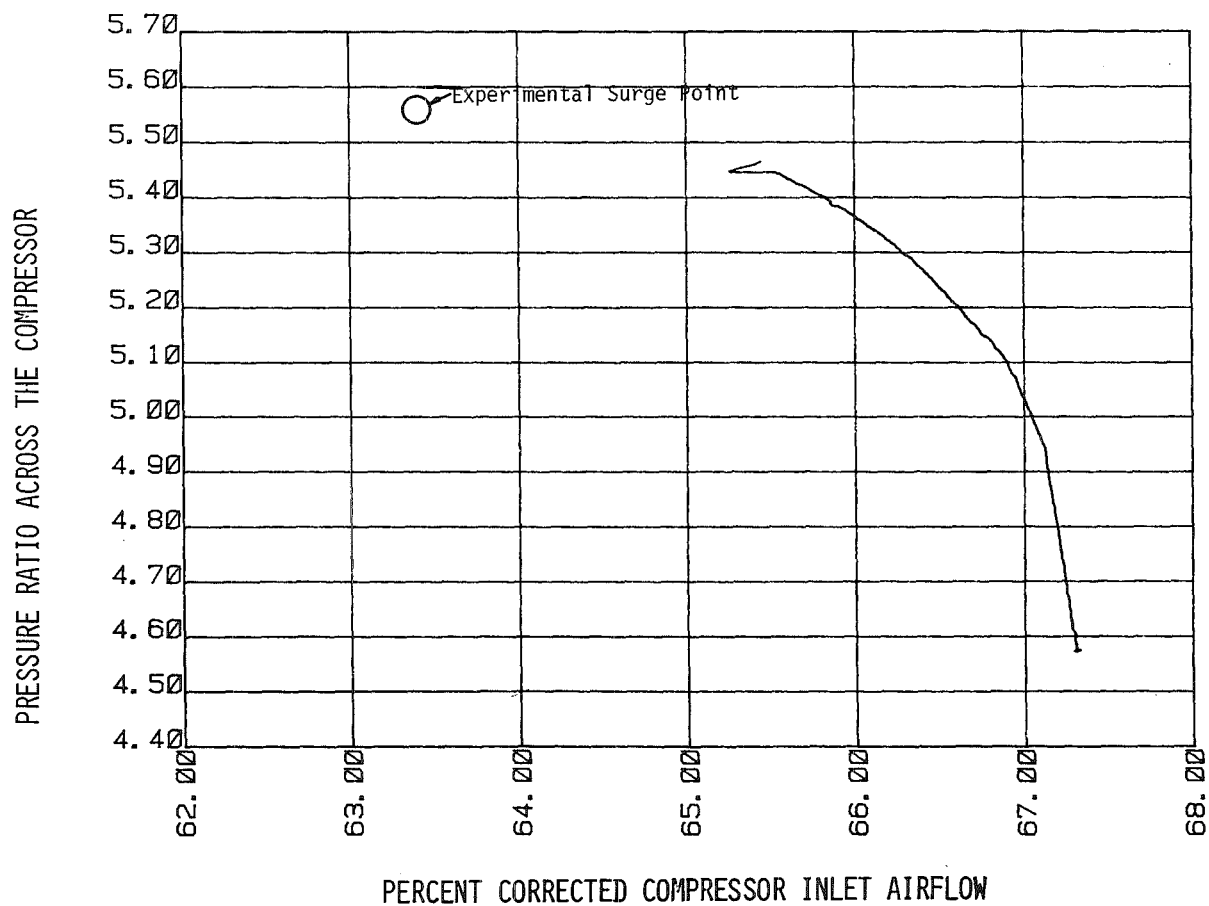


Figure 4. Model prediction of the compressor performance under loading till surge point at 87 percent corrected speed (Runge-Kutta Scheme).

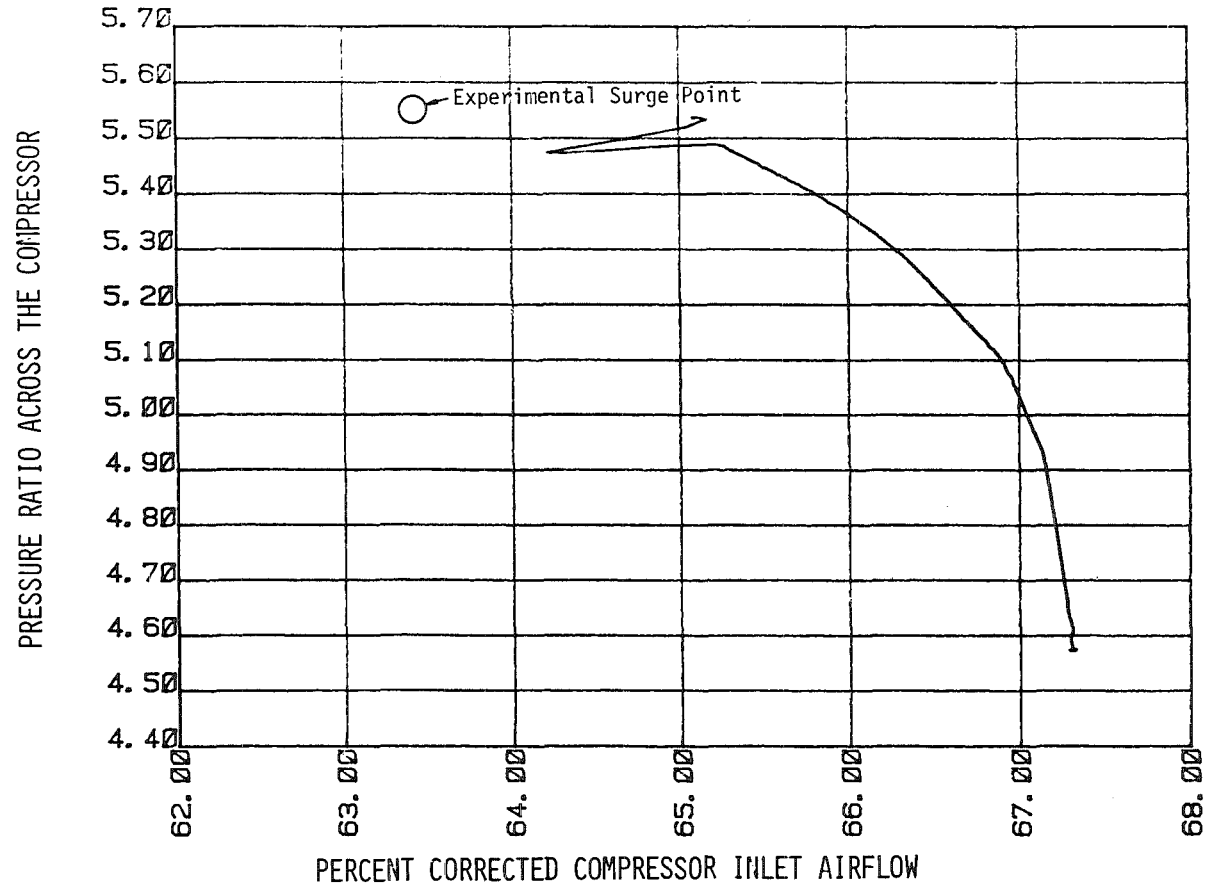


Figure 5. Model prediction of the compressor performance under loading till surge point at 87 percent corrected speed (JRS Scheme).

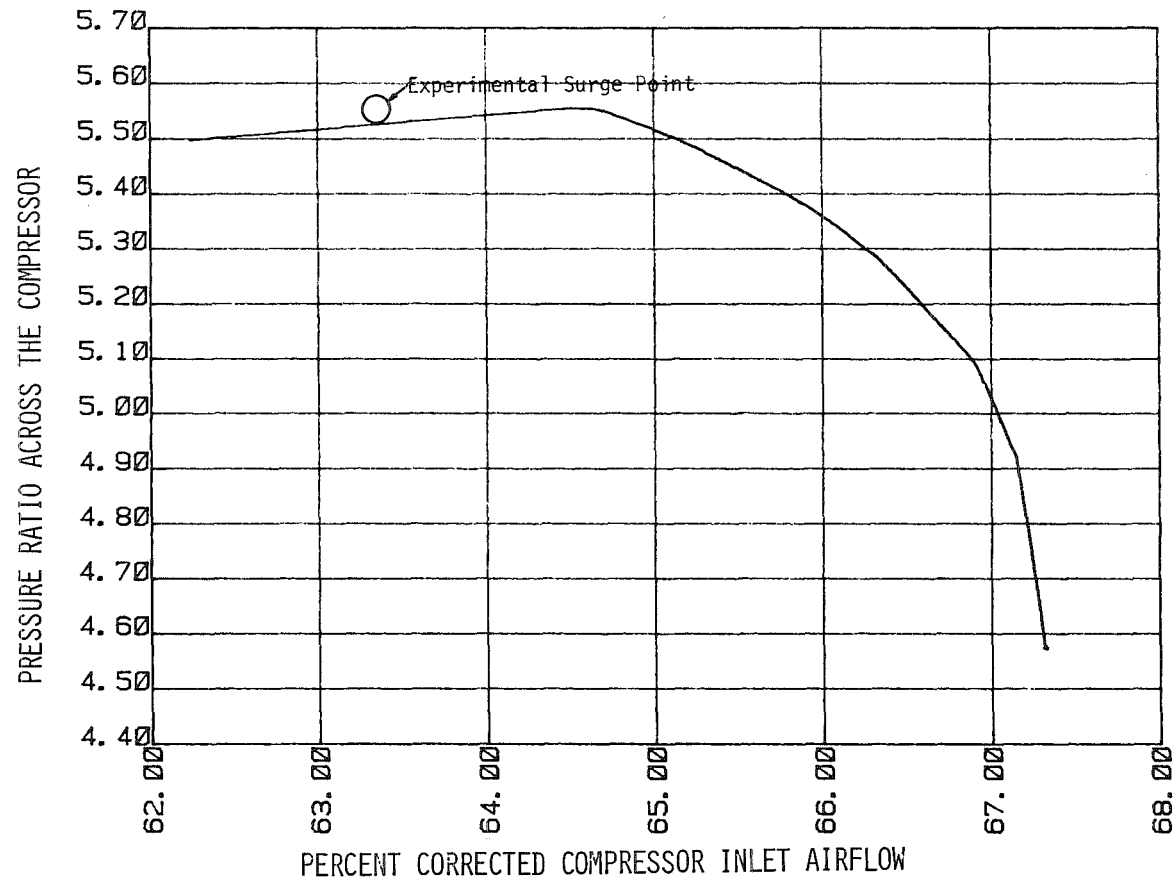


Figure 6. Model prediction of the compressor performance under loading till surge point at 87 percent corrected speed (MacCormack Scheme).

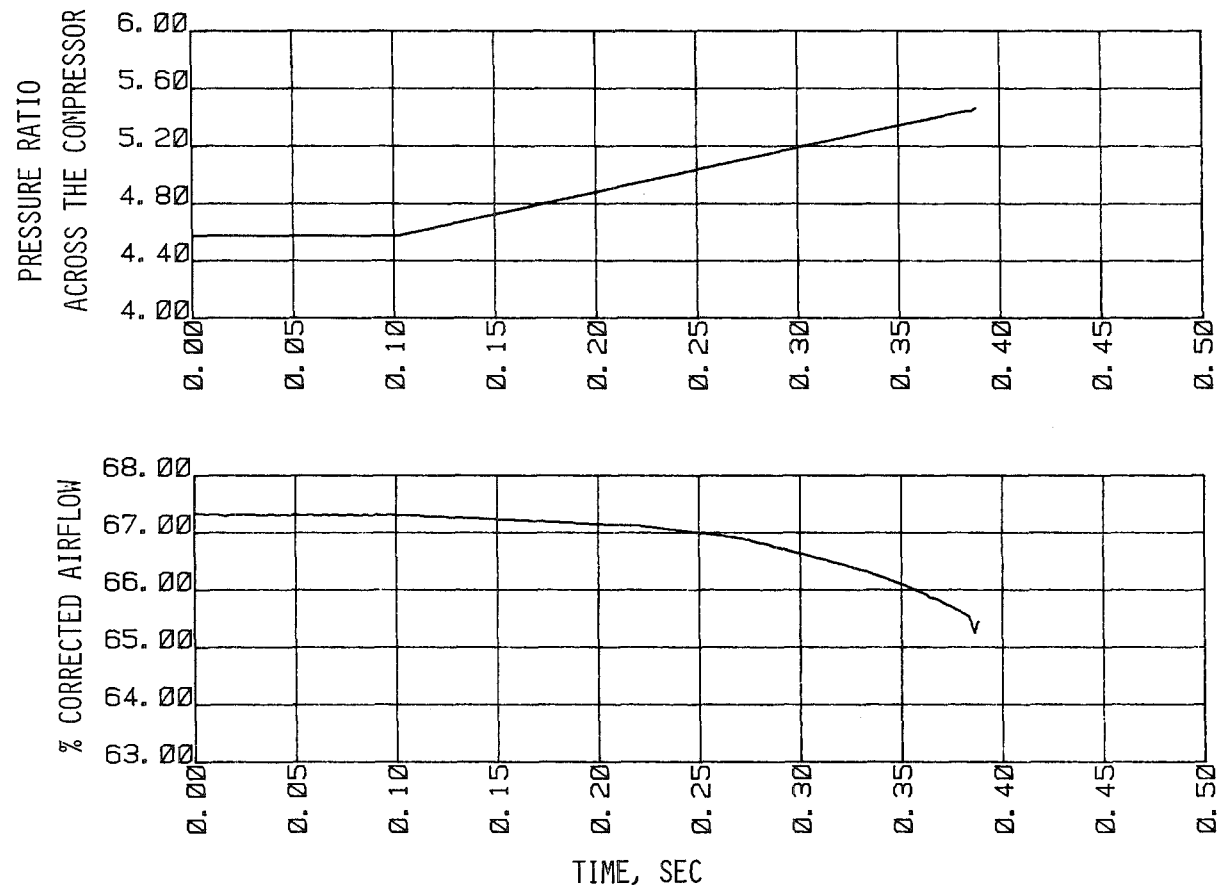


Figure 7. Variation of the compressor flow parameters with time till surge point - 87 percent corrected speed (Runge-Kutta Scheme).

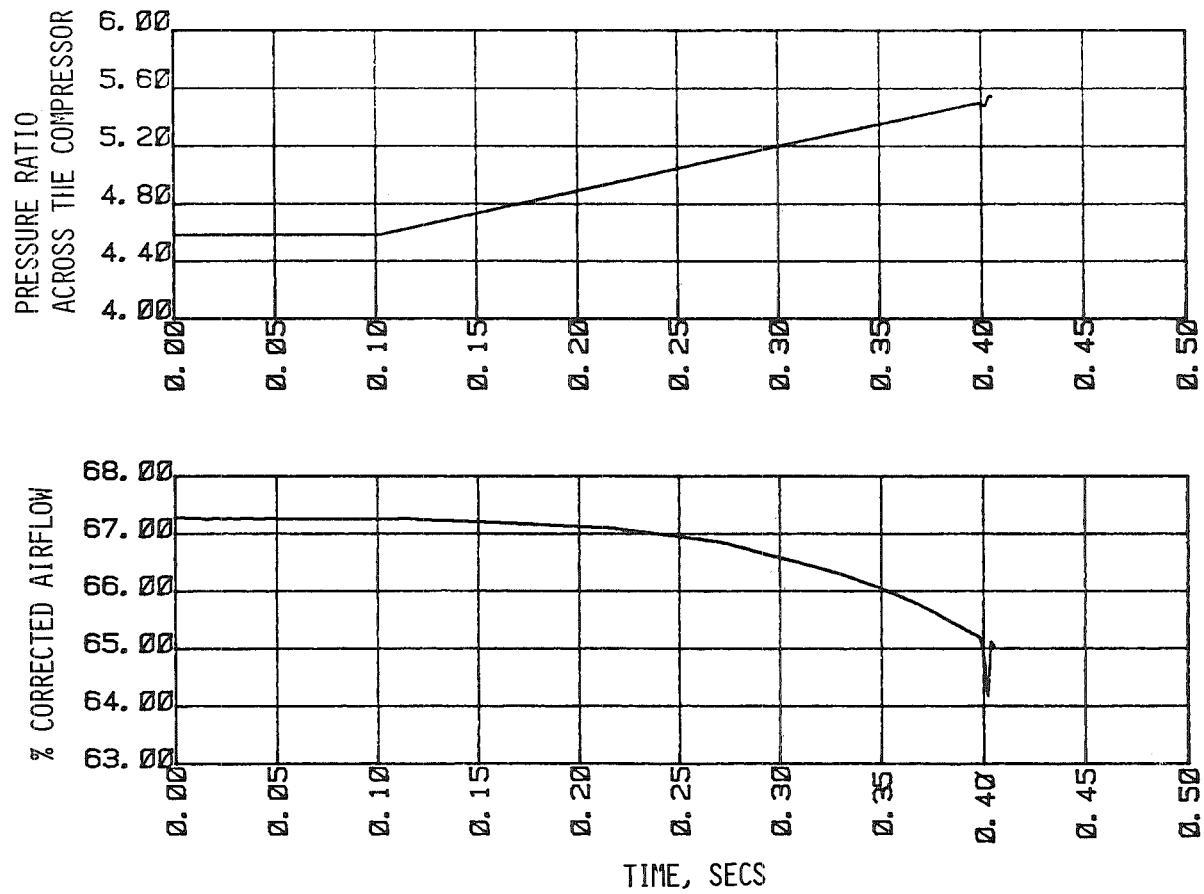


Figure 8. Variation of the compressor flow parameters with time till surge point - 87 percent corrected speed (JRS Scheme).

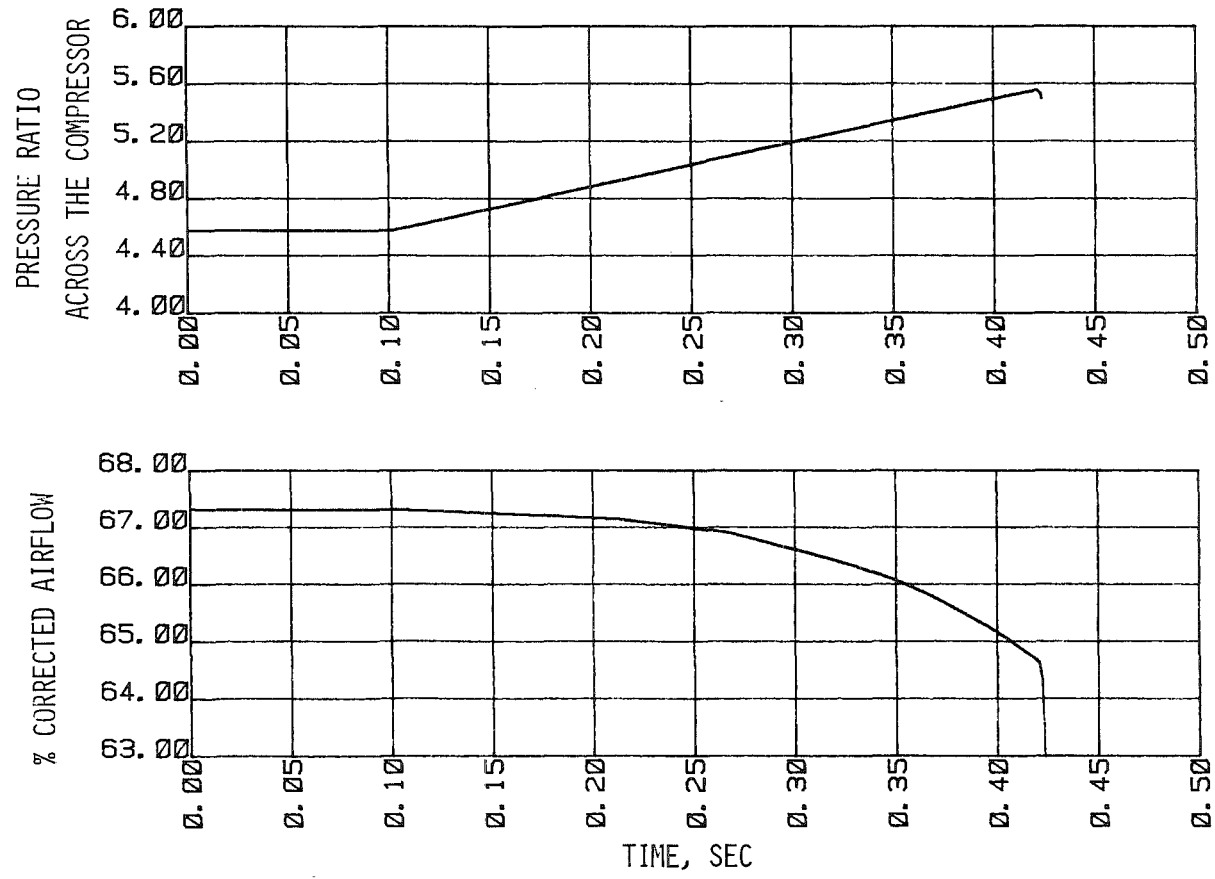


Figure 9. Variation of the compressor flow parameters with time till surge point – 87 percent corrected speed (MacCormack Scheme).

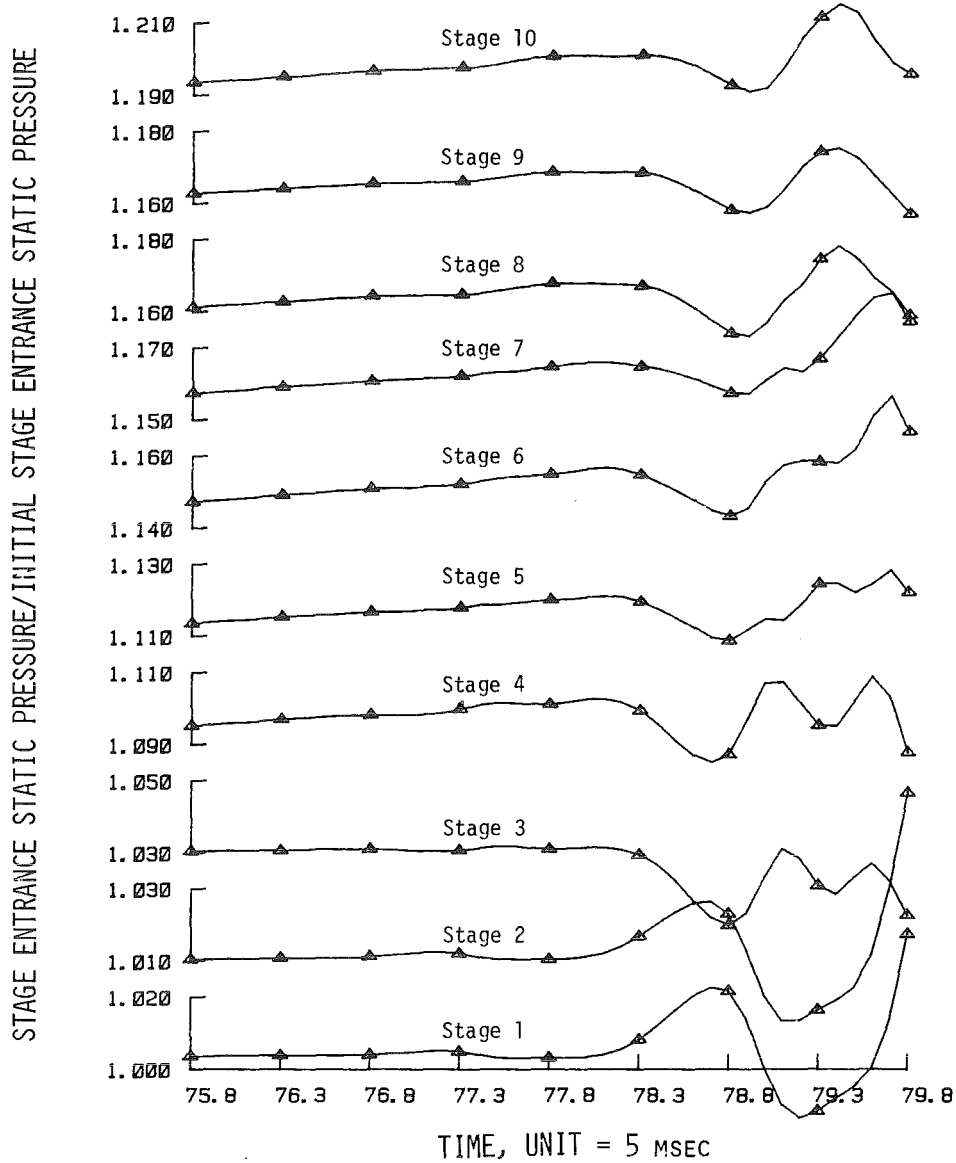


Figure 10. Individual stage pressure variations just before surge - 87 percent corrected speed (Runge-Kutta Scheme).

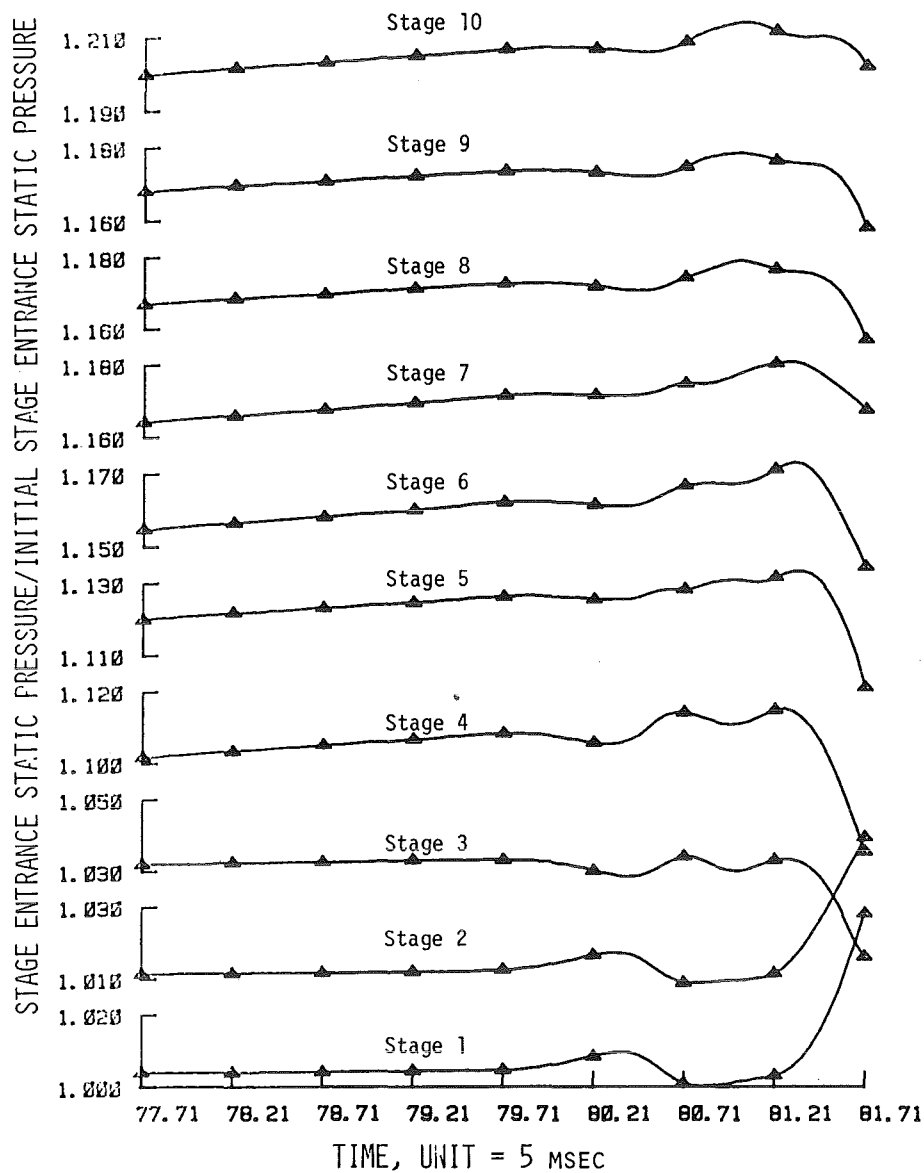


Figure 11. Individual stage pressure variations just before surge - 87 percent corrected speed (JRS Scheme).

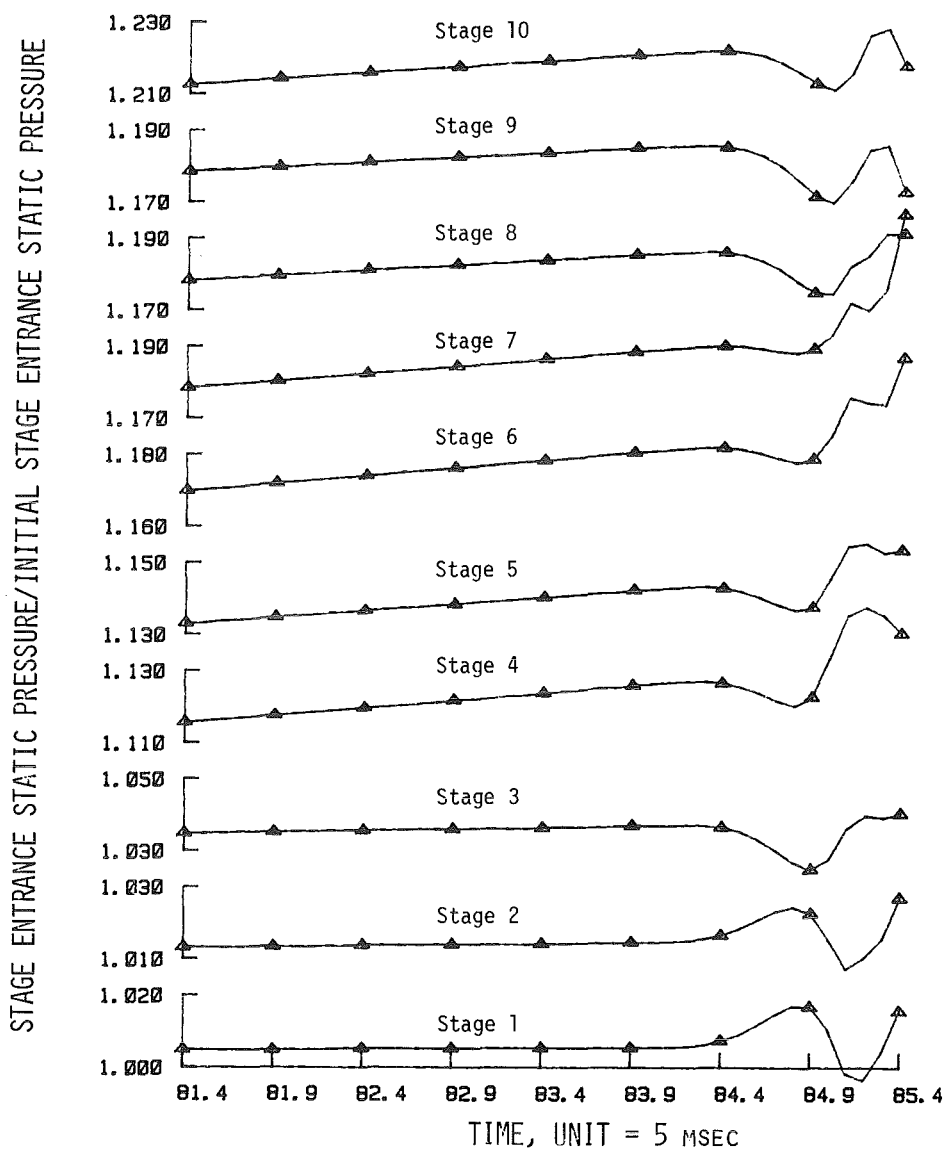


Figure 12. Individual stage pressure variations just before surge - 87 percent corrected speed (MacCormack Scheme).

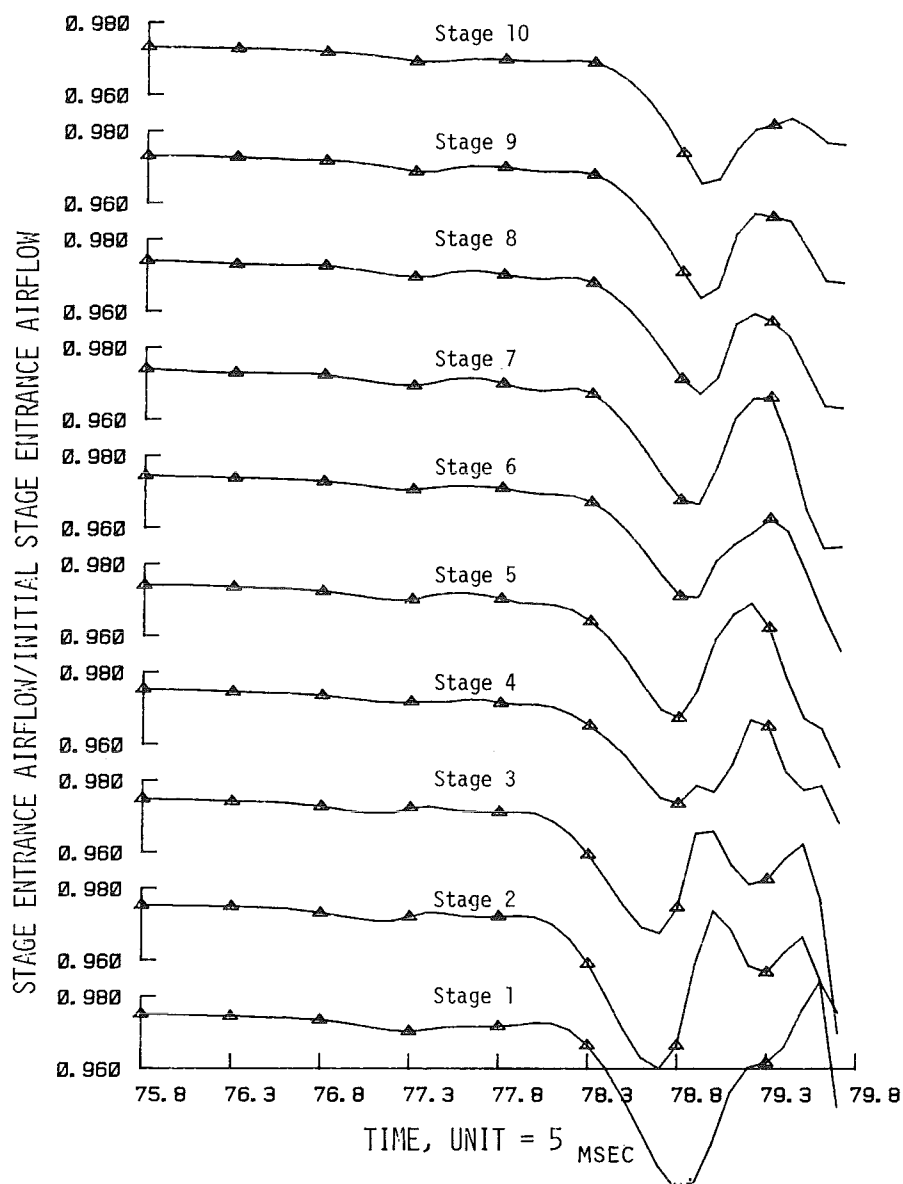


Figure 13. Individual stage airflow variations just before surge - 87 percent corrected speed (Runge-Kutta Scheme).

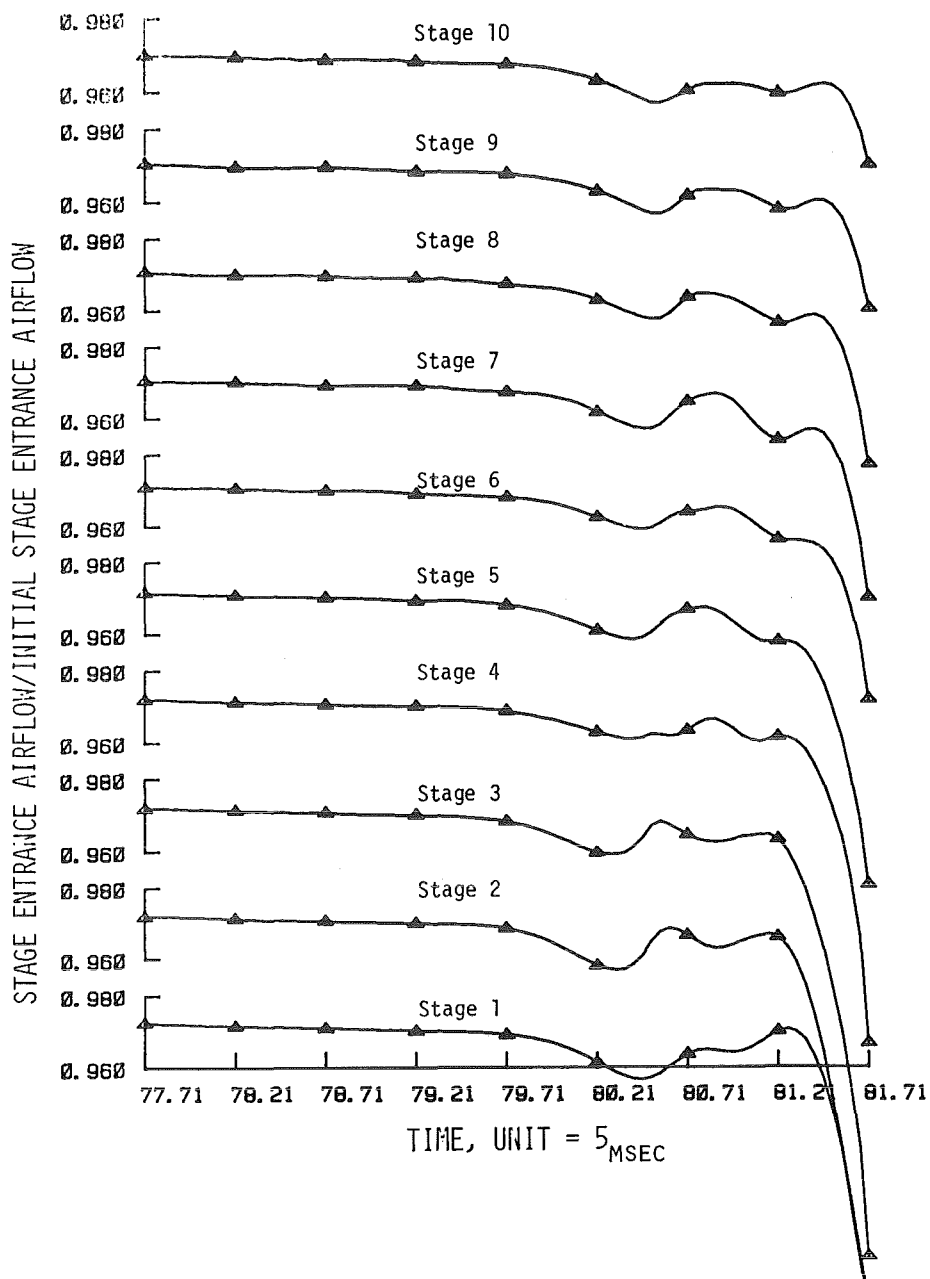


Figure 14. Individual stage airflow variations just before surge - 87 percent corrected speed (JRS Scheme).

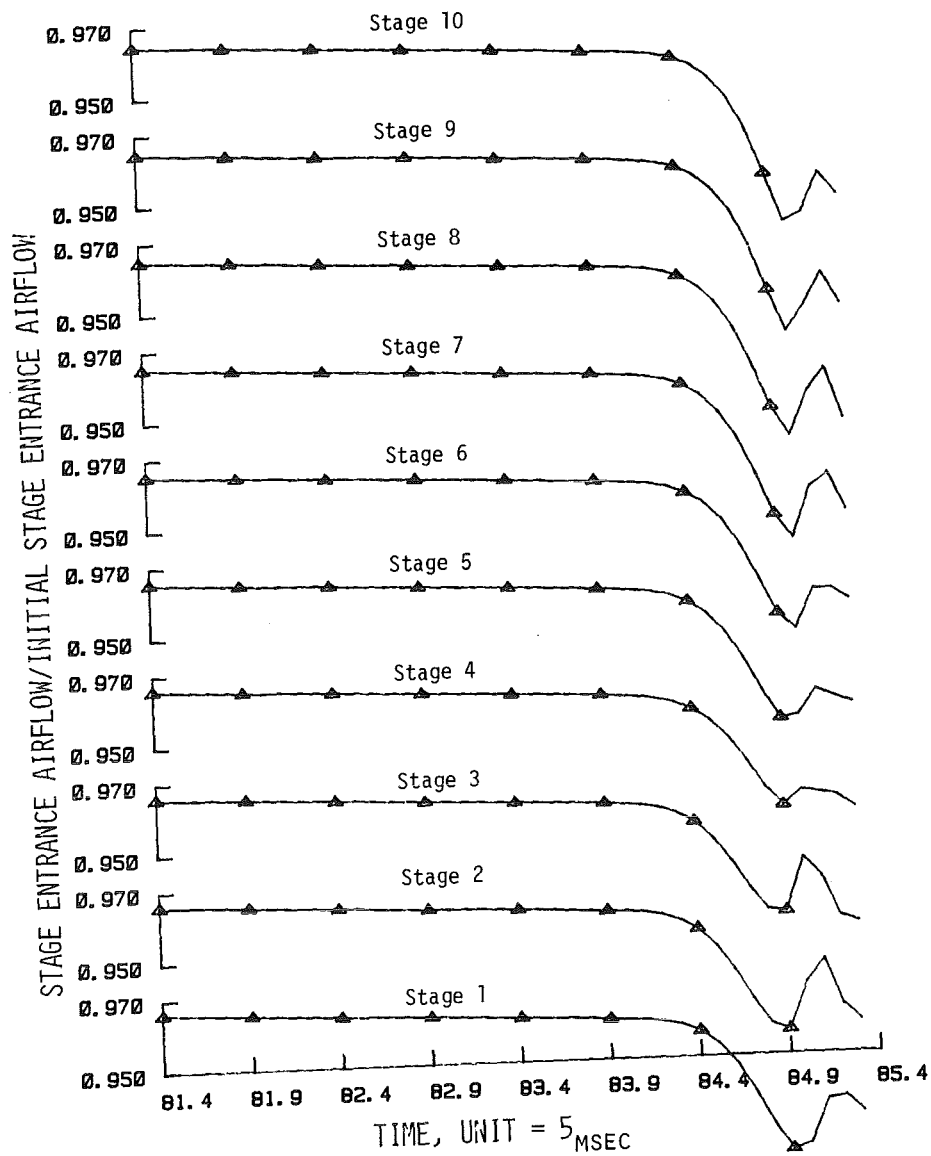


Figure 15. Individual stage airflow variations just before surge - 87 percent corrected speed (MacCormack Scheme).

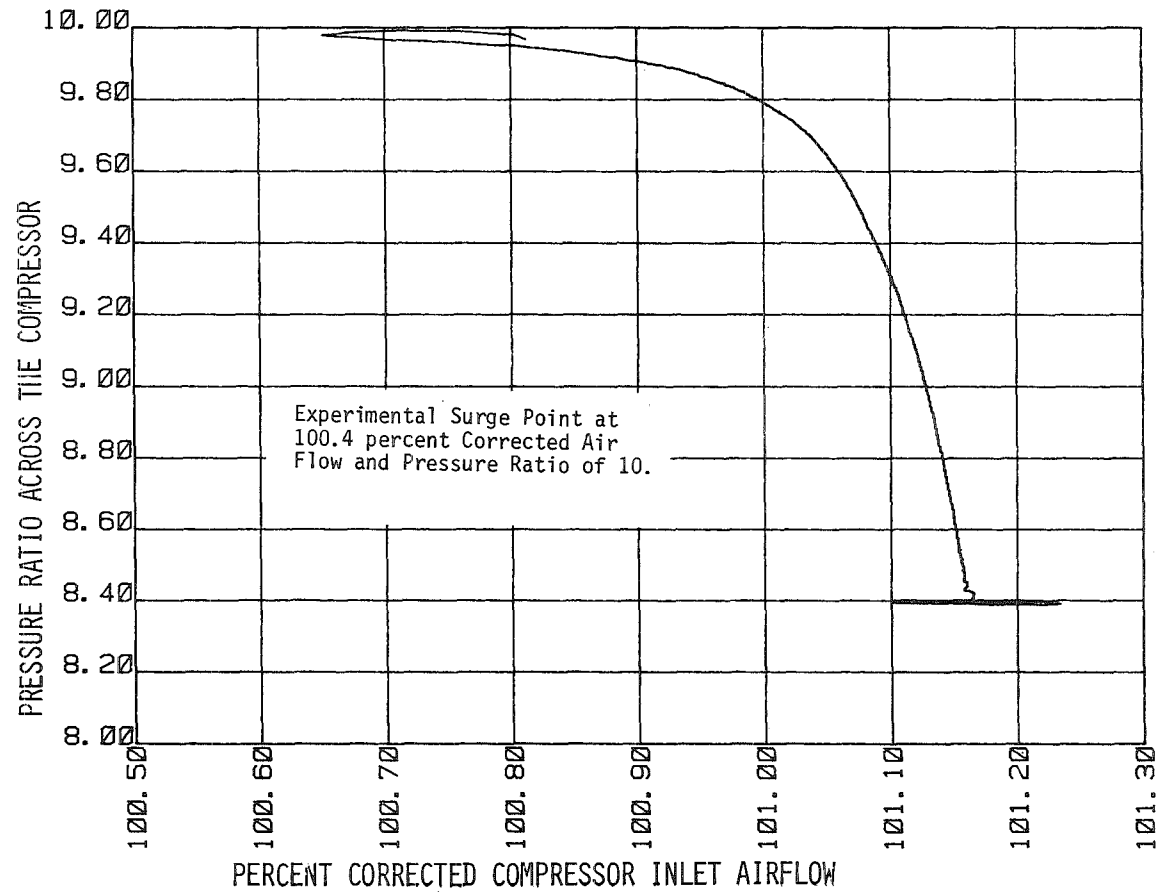


Figure 16. Model prediction of the compressor performance under loading till surge point at 102 percent corrected speed (Runge-Kutta Scheme).

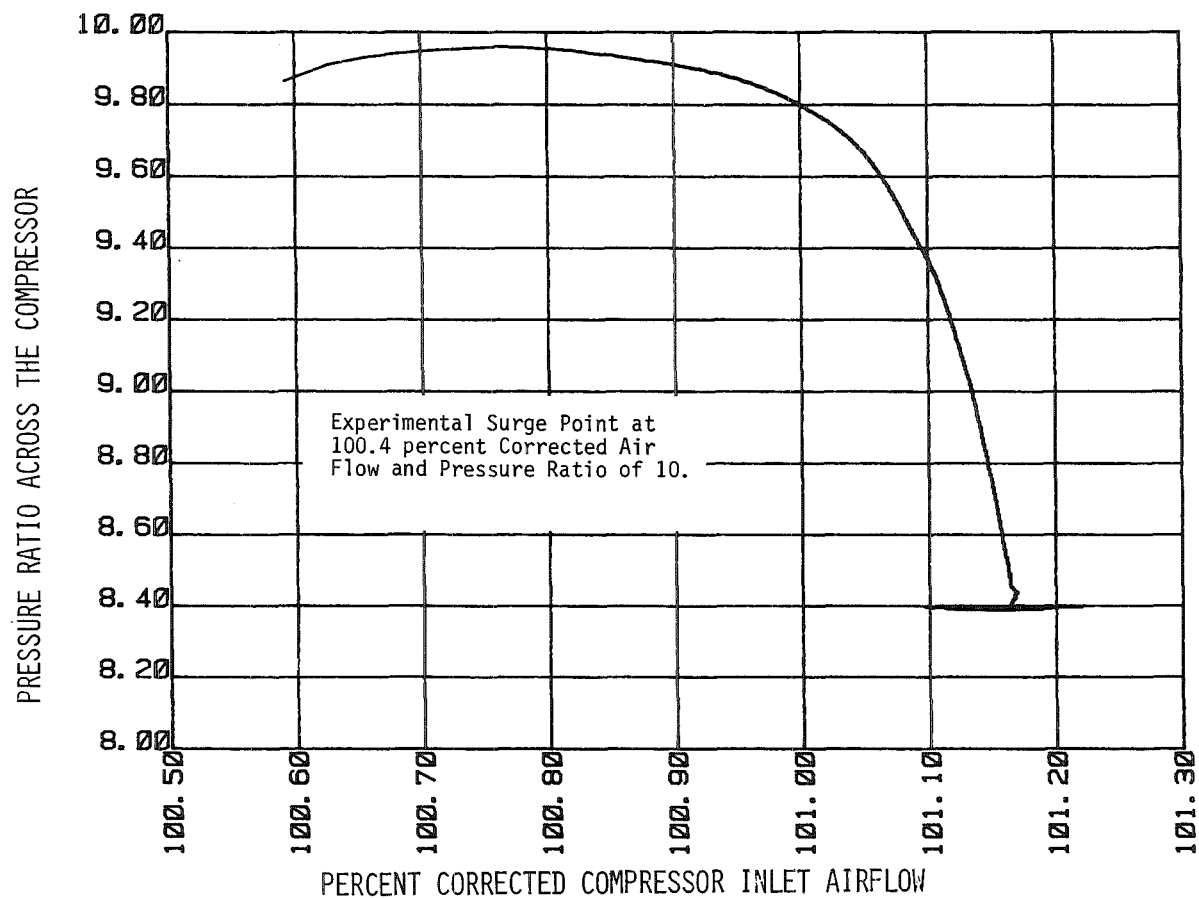


Figure 17. Model prediction of the compressor performance under loading till surge point at 102 percent corrected speed (JRS Scheme).

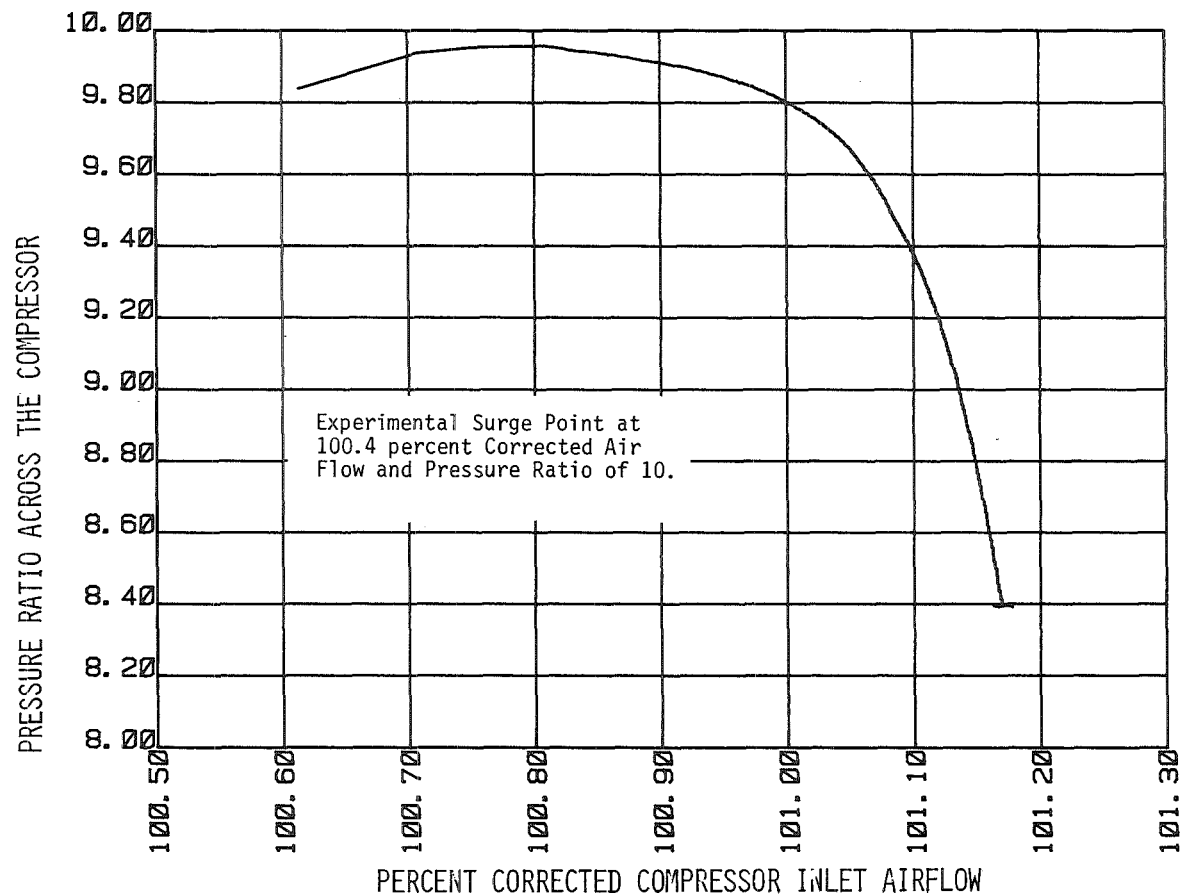


Figure 18. Model prediction of the compressor performance under loading till surge point at 102 percent corrected speed (MacCormack Scheme).

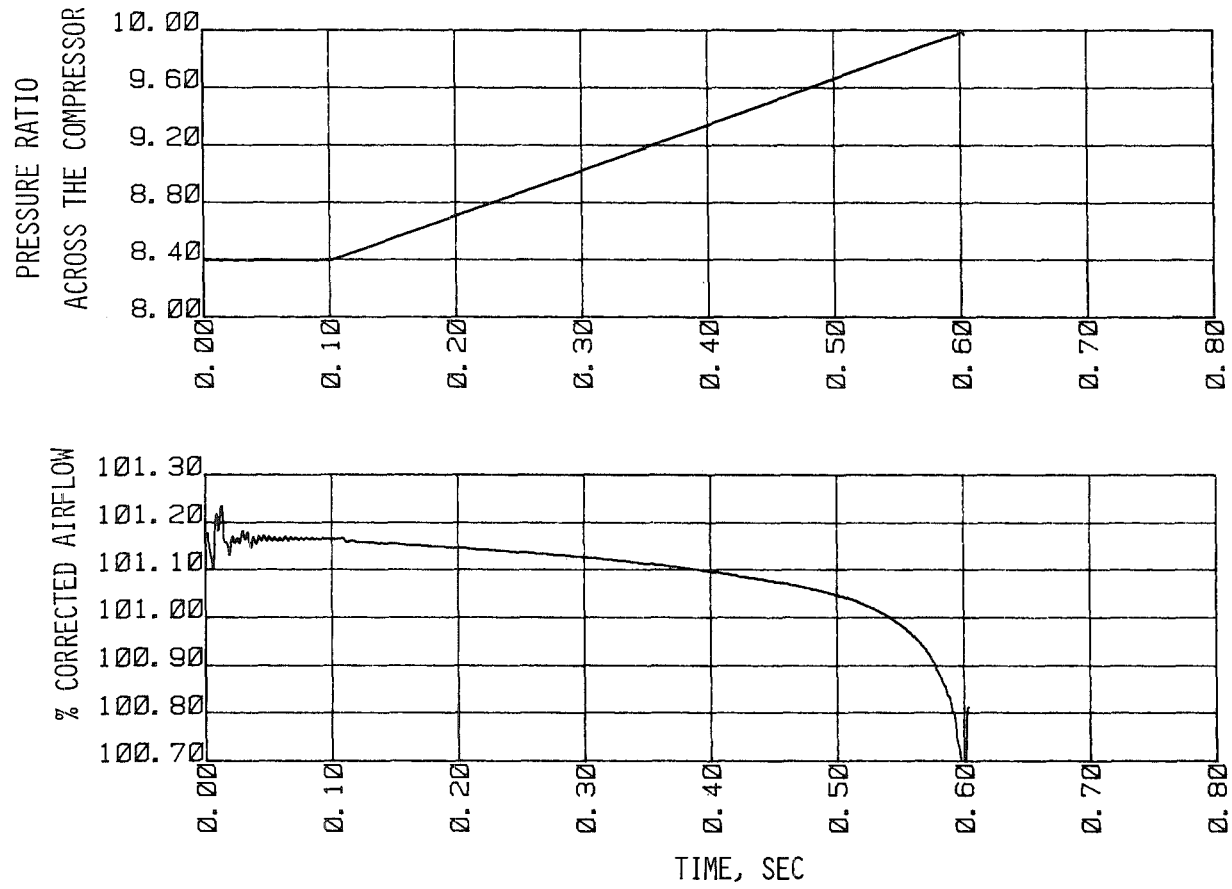


Figure 19. Variation of the compressor flow parameters with time till surge point - 102 percent corrected speed (Runge-Kutta Scheme).

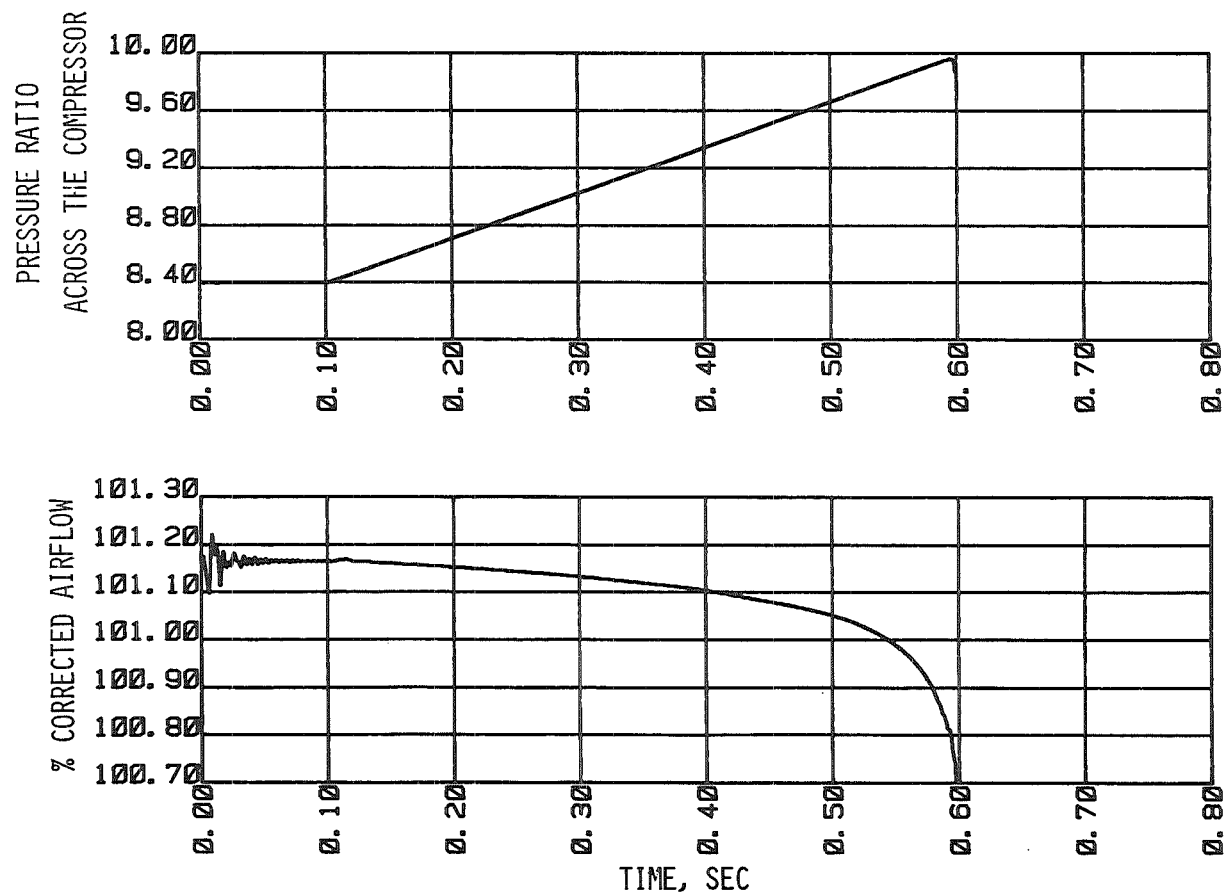


Figure 20. Variation of the compressor flow parameters with time till surge point - 102 percent corrected speed (JRS Scheme).

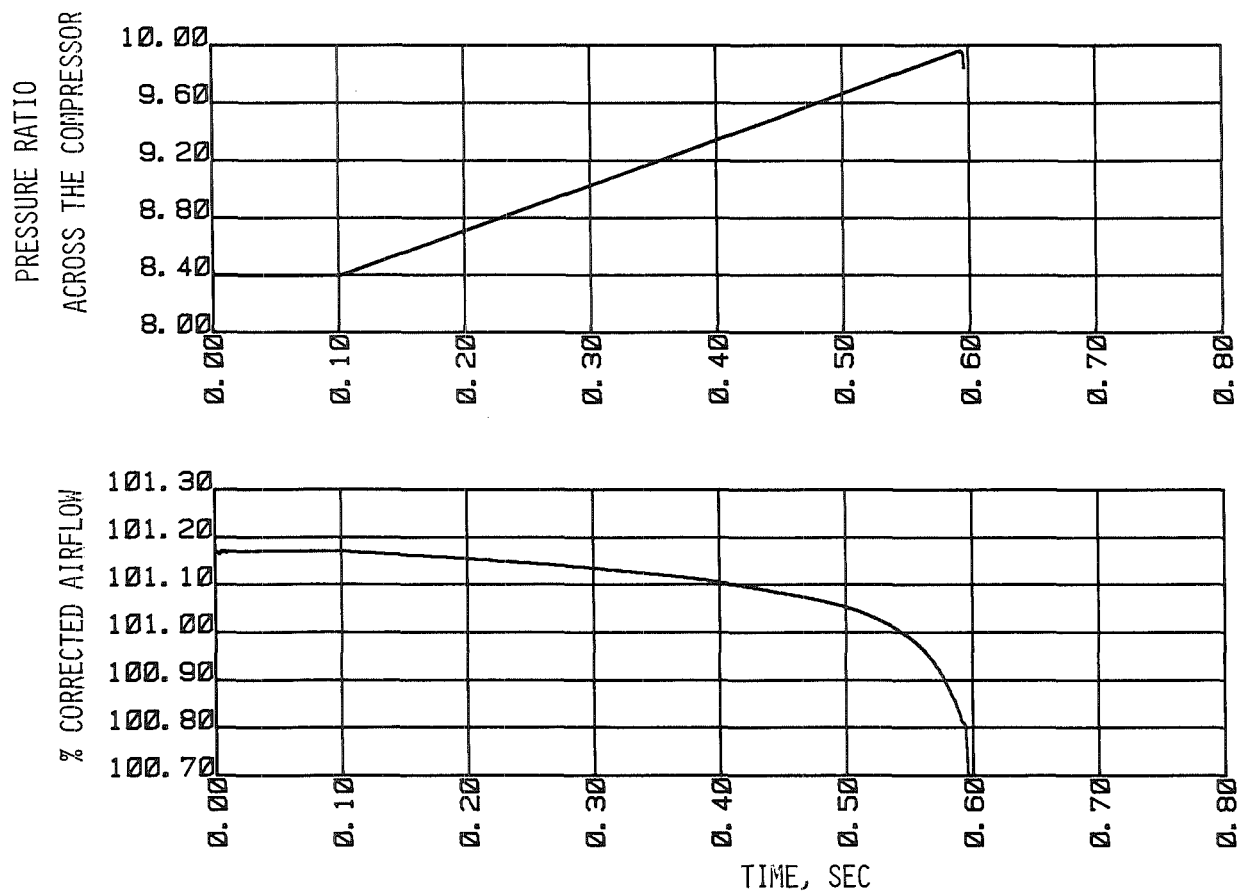


Figure 21. Variation of the compressor flow parameters with time till surge point - 102 percent corrected speed (MacCormack Scheme).

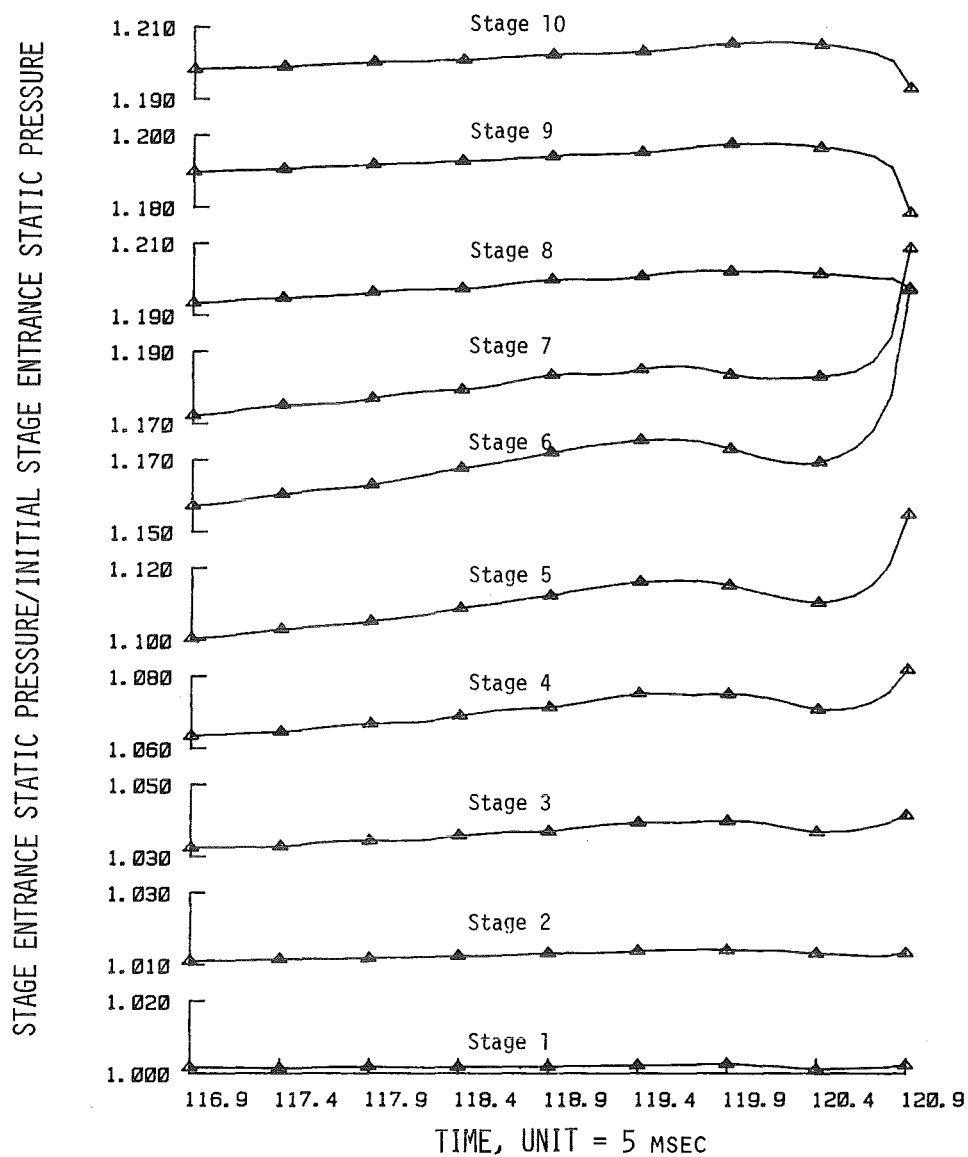


Figure 22. Individual stage pressure variations just before surge - 102 percent corrected speed (Runge-Kutta Scheme).

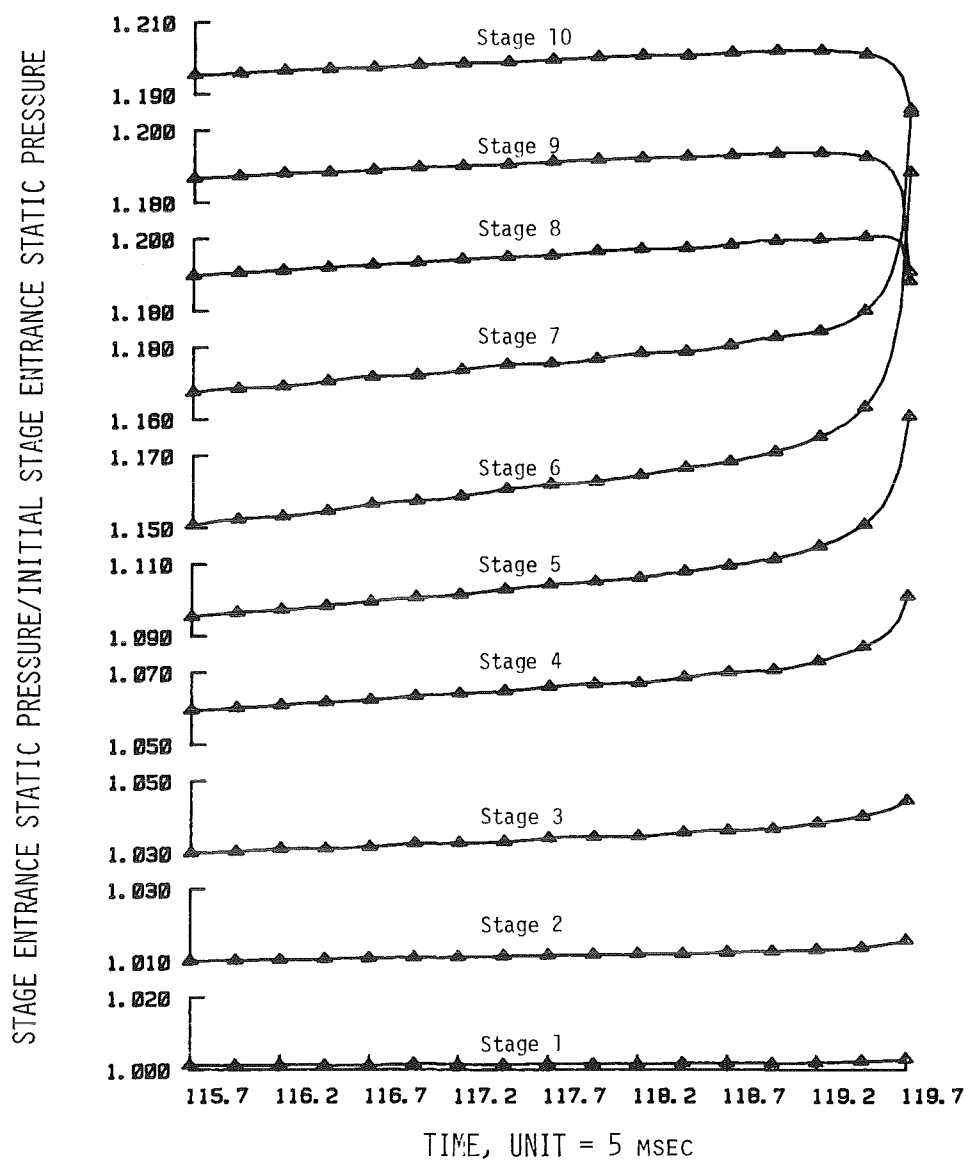


Figure 23. Individual stage pressure variations just before surge - 102 percent corrected speed (JRS Scheme).

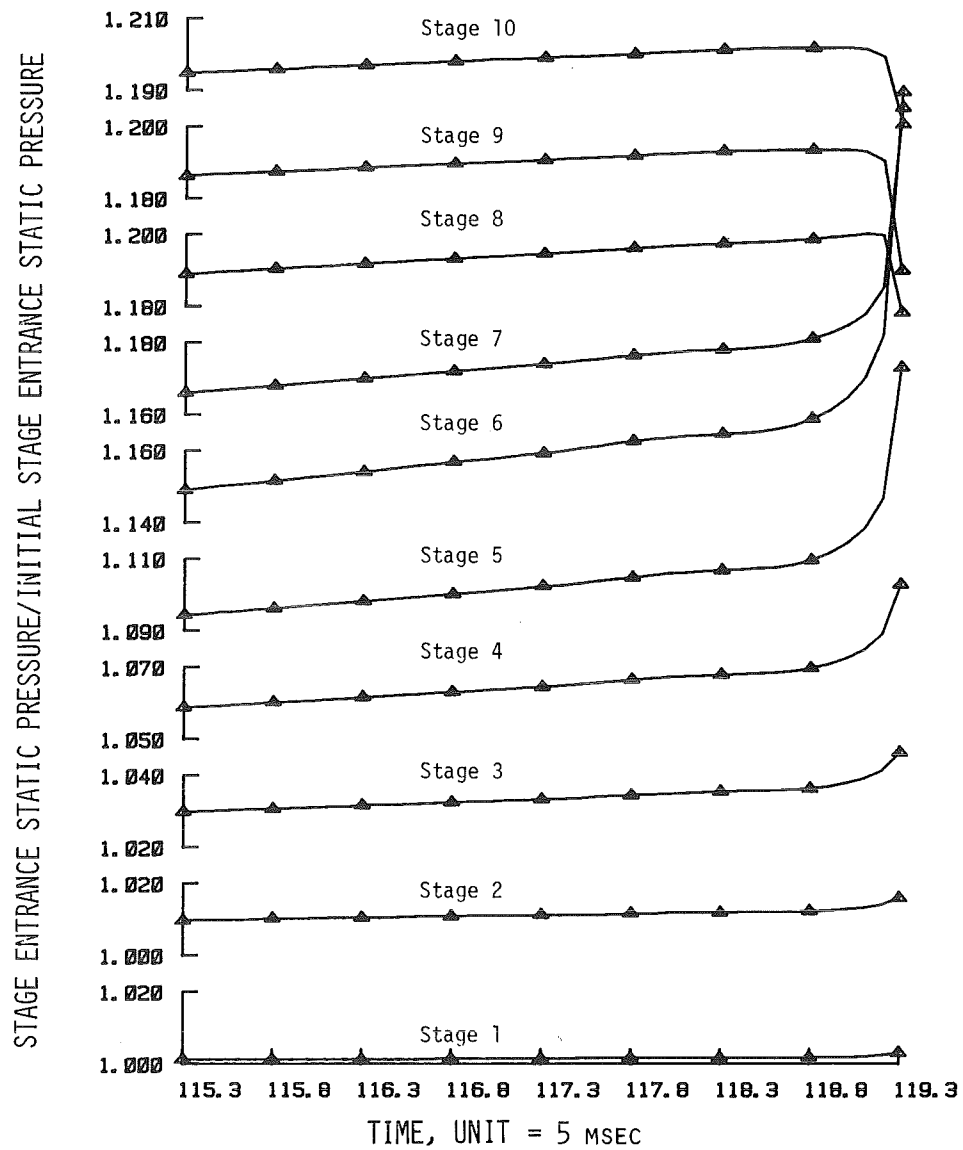


Figure 24. Individual stage pressure variations just before surge - 102 percent corrected speed (MacCormack Scheme).

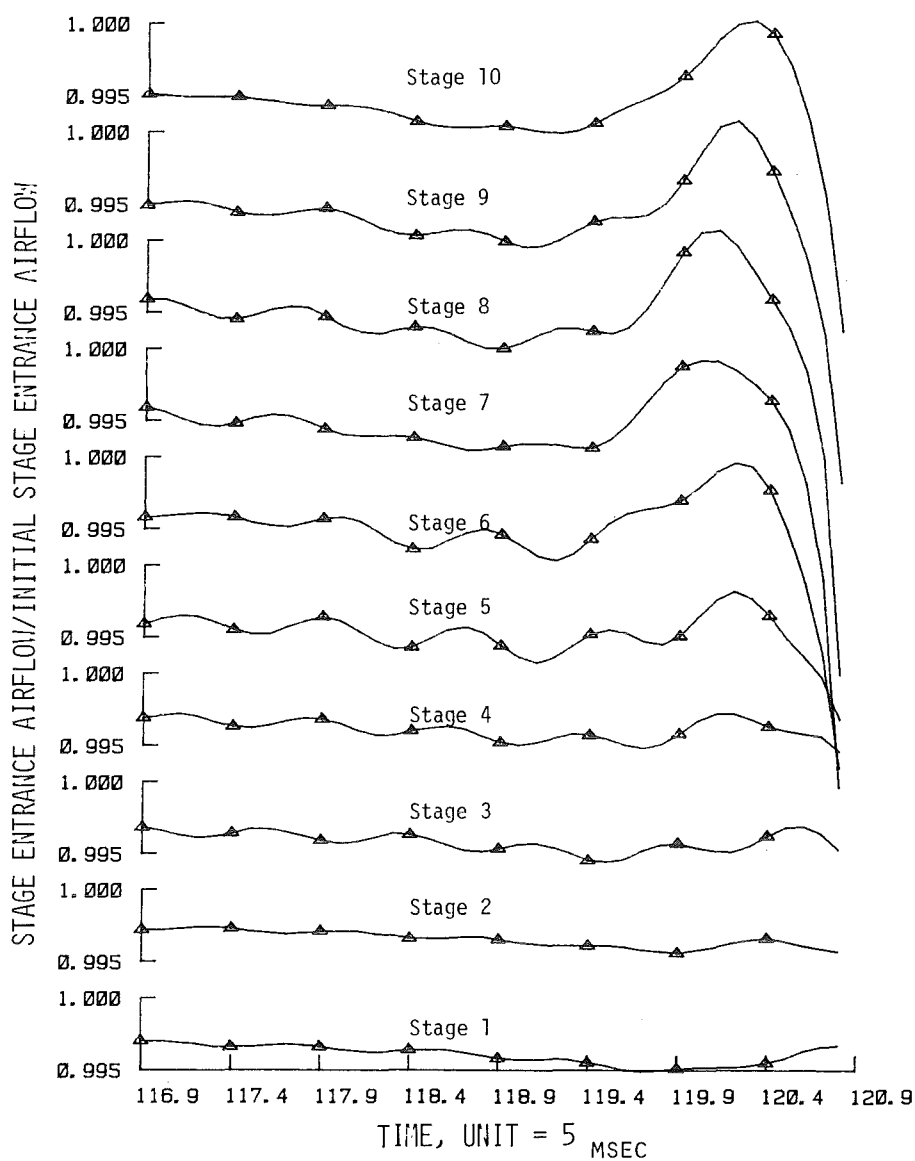


Figure 25. Individual stage airflow variations just before surge - 102 percent corrected speed (Runge-Kutta Scheme).

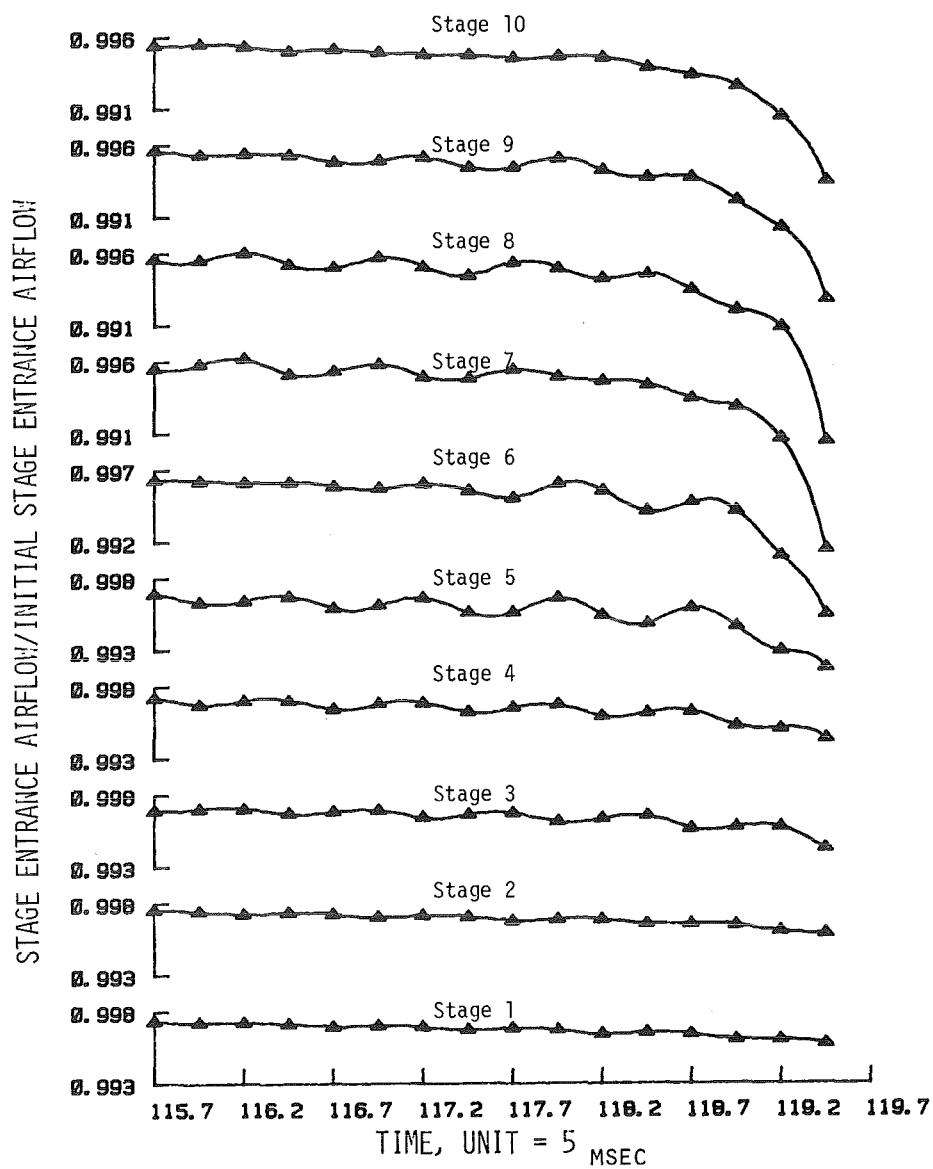


Figure 26. Individual stage airflow variations just before surge - 102 percent corrected speed (JRS Scheme).

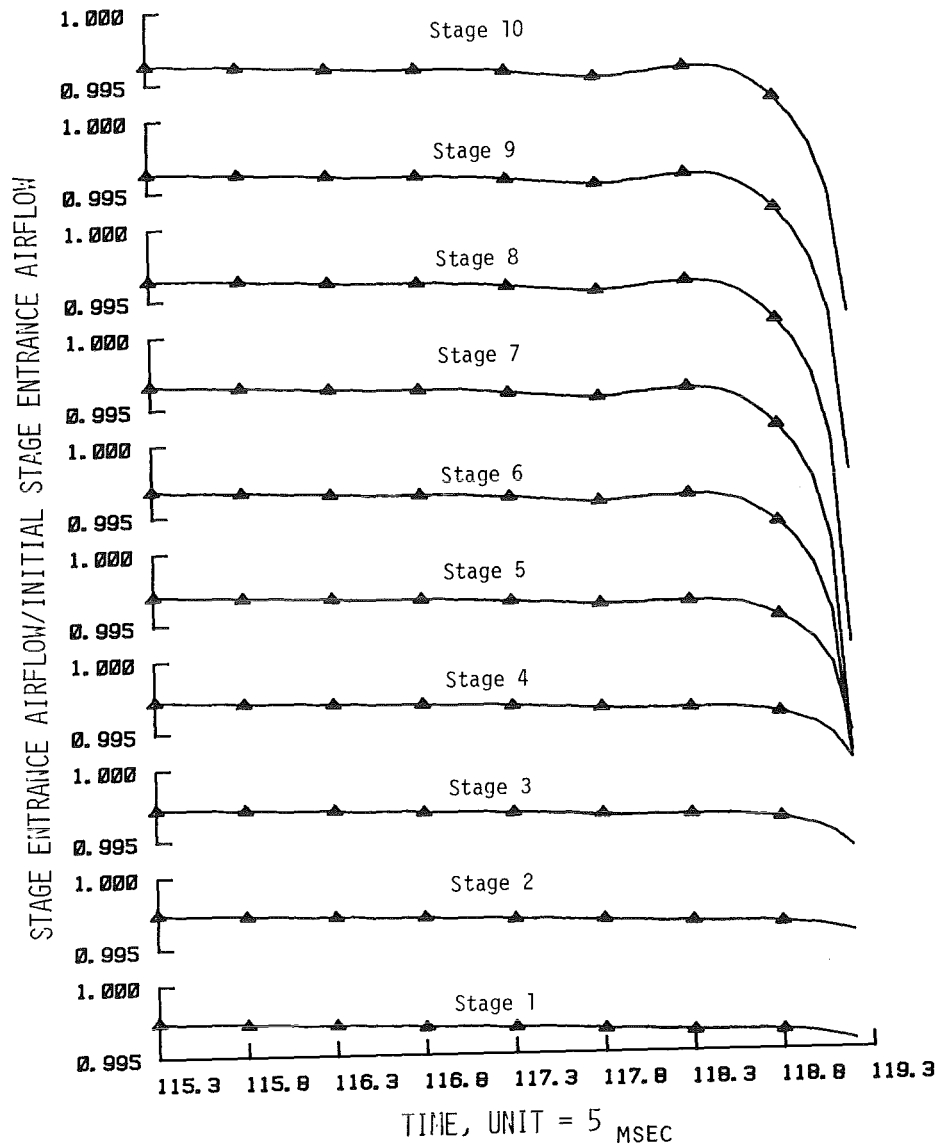


Figure 27. Individual stage airflow variations just before surge - 102 percent corrected speed (MacCormack Scheme).